A New Type of Emerald from Afghanistan's Panjshir Valley

Michael S. Krzemnicki, Hao A. O. Wang and Susanne Büche

ABSTRACT: Since 2017, a new type of emerald from the Panjshir Valley, Afghanistan, has entered the gem trade. This material is commonly of excellent quality and compares with the finest emeralds from Colombia, not only visually, but also with respect to inclusions, spectral features and chemical composition. As a result, some of these stones have entered the market as Colombian emeralds. This study presents detailed microscopic, spectral and trace-element data for these recently produced Afghan emeralds and compares them to 'classic' emeralds from the Panjshir Valley and from Laghman Province in Afghanistan. The samples from each of the three Afghan occurrences showed differences in their UV-Vis-NIR spectra and water-related features in their Raman spectra, and they could also be distinguished from one another—as well as those from other important emerald deposits worldwide— by their trace-element composition. A distinctly higher Fe concentration is the main criterion that separates the recent Panjshir production from Colombian emeralds. This study further shows that it is possible to clearly differentiate emeralds from different localities based on trace-element data using t-SNE statistical processing, which is an unsupervised machine-learning method.

Emerald, the green chromium-bearing variety of beryl ($Be_3Al_2Si_6O_{18}$), has been one of the most sought-after gem materials throughout history. Since the 17th century, emeralds from Colombia have gained the highest reputation and market importance, but other sources have also emerged in recent decades, such as Zambia (e.g. Kafubu), Madagascar (e.g. Mananjary) and Ethiopia (Shakiso) in Africa, as well as Pakistan (Swat Valley), Afghanistan (Panjshir [Panjsher] Valley) and China (Davdar in the Xinjiang Uyghur Autonomous Region) in Asia. Stones from the Panjshir Valley in Afghanistan are commonly described as resembling Colombian emeralds in terms of colour, quality and even inclusion features (Bowersox *et al.* 1991; Schwarz & Pardieu 2009). Their reputation is underscored by the fact that a 10 ct Afghan emerald was sold at auction in 2015 for USD2.275 million (Christie's 2015)—equivalent to the highest recorded per-carat price for any emerald from a non-Colombian locality.

The Swiss Gemmological Institute SSEF regularly receives emeralds from Afghanistan for testing, quite often in impressive layouts and settings. In the past, determining their geographic origin was in most cases quite straightforward. However, in early 2017 this changed, and since then we have analysed more than 100 samples of an apparently new type of emerald from the Panjshir Valley in Afghanistan. (Hereafter in this article these stones will be referred to as 'Panjshir type II' emeralds.) They have been submitted to SSEF by reliable sources for research and testing, and currently we do not have any further information on the specific mining area in the Panjshir Valley that produced them. However, based on their uniform appearance and exceptional quality, as well as their consistent inclusion features and very homogeneous chemical composition, the authors assume that they originated from a specific Panjshir location (or gem 'pocket') and not from various mining sites within the area. The stones

more closely resemble Colombian emeralds in terms of inclusion features, physical properties and trace-element concentrations (Krzemnicki 2018), as compared to the previously known material from Afghanistan (hereafter referred to as 'Panjshir type I' emeralds). Because the Panjshir type II stones are often of very high quality—matching the best Colombian emeralds from Muzo and other famous Colombian mines—this makes accurate origin attribution even more important.

In this study, we present detailed gemmological data for Panjshir type II emeralds and compare them to previously known emeralds from Afghanistan (from Panjshir and Laghman Province; Figure 1). In addition, we compare the Panjshir type II emeralds to those from other deposits, including Colombia, with the aim of providing reliable criteria for origin determination.

LOCATION AND GEOLOGY

Emeralds from Afghanistan's Panjshir Valley have been traded for an unknown period of time. Theophrastus's *Treatise on Stones* (314 BC; see Forestier & Piat 1998) and Pliny the Elder's *Naturalis* (77 AD; see Bowersox *et al.* 1991) both mentioned *smaragdus* from Bactria, much of which lay in modern-day Afghanistan. However, *smaragdus* was also used in antiquity to describe a wide range of green gems, so it is uncertain whether these reports refer to emeralds from Afghanistan. Interestingly, oxygen isotope analysis of a historic emerald from the treasure of Nizam in Hyderabad (India) revealed that the Panjshir Valley was its likely origin (Giuliani *et al.*

2000). This evidence supports Panjshir as a (sporadic) source of gem-quality emeralds at least as early as the 18th century.

In the modern gem market, Panjshir emeralds have been known since the 1970s (Bariand & Poullen 1978). Systematic surveys were done by Russian and Afghan geologists (Rossovskiy *et al.* 1976; Abdullah *et al.* 1977; Rossovskiy 1981; Chmyriov *et al.* 1982), and the deposits were also described in a few gemmological publications (Bowersox 1985; Bowersox *et al.* 1991). Years later, emeralds were also discovered in neighbouring Laghman Province, including some gem-quality material near the village of Korgun (about 100 km east of Kabul) and semi-transparent stones near Lamonda (Laurs 2001; Henn & Schmitz 2014; Groat *et al.* 2014).

Today, the mines of the Panjshir Valley (literally 'Valley of the Five Lions') are the main source of gem-quality emeralds in Afghanistan. The largest specimens reported in the literature are an 8 g crystal (Sultan & Aria 2018) and a 15 ct faceted stone (Schwarz & Giuliani 2002). However, in the past two decades, the authors have seen and tested fine-quality Afghan emerald crystals larger than 120 g and faceted stones over 85 ct. Nevertheless, based on our lab experience, most gem-quality faceted emeralds from Afghanistan are less than 5 ct. By comparison, the Panjshir type II emeralds that emerged since 2017 are generally rather small (median about 2.5 ct), but in rare cases they reach up to 20 ct.

The Panjshir Valley is located about 150 km north-east of Kabul in the Hindu Kush mountain range and follows the Panjshir River north-east to south-west (Figure 2).

Figure 1: The three types of emeralds from Afghanistan discussed in this article are illustrated here: a 10.11 ct Panjshir type I emerald of very fine quality that was also set in the ring shown on the cover of this issue (left), a 2.42 ct Panjshir type II emerald of excellent quality (centre) and an 18.58 ct Laghman-type emerald (right). Photos by Luc Phan; composited by M. S. Krzemnicki, © SSEF.

Figure 2: The map on the left (© USAID) shows the location of the emerald deposits in the Panjshir Valley and near Korgun (Laghman Province) in north-east Afghanistan. The three-dimensional block map on the right (courtesy of WikiCommons) is looking into the Panjshir Valley, which extends about 100 km towards the north-east. The Panjshir emerald mining area is located upstream of Khenj village, which is about 115 km from Kabul.

The emerald mines are located in a zone approximately 16 km long and 3 km wide extending north-east along the Panjshir River from Khenj village (Bowersox *et al.* 1991; Giard 1998), at elevations of about 2000–4000 m (DeWitt *et al.* 2020).

The Panjshir Valley follows a continental collision zone—the Herat-Panjshir suture (Chmyriov *et al.* 1982; Kazmi & Snee 1989; Giuliani *et al.* 2019)—which divides platform-derived sedimentary rocks in northern Afghanistan from southern structural blocks of various origins (Bowersox 2015) that also contain metamorphosed relics of the Paleo-Tethys Ocean (Bowersox *et al.* 1991; Snee *et al.* 2005).

The emerald deposits are found in Proterozoic metamorphic basement rocks consisting of migmatite, gneiss, schist, marble and amphibolite. They are classified as type IIC (tectonic-metamorphic-related deposits, and hosted in metamorphic rocks; Giuliani *et al.* 2019). The emeralds formed within vugs and quartz veins, and are associated with muscovite, tourmaline, albite, pyrite, rutile, dolomite and chlorapatite in schists that were affected by intense fracturing, fluid circulation and hydrothermal alteration (Sabot *et al.* 2000; Groat *et al.*

2014; Giuliani *et al.* 2019). Similar to Colombian emeralds, Panjshir material contains fluid inclusions of high salinity, which indicates (as in Colombia) a leaching of evaporite sequences (Giuliani *et al.* 1997, 2017; Sabot *et al.* 2000) by hydrothermal alteration during the Himalayan orogeny. In contrast to Colombian emeralds, however, they formed at a distinctly higher metamorphic grade, at around 400°C (Schwarz & Giuliani 2002) during Oligocene time. (^{40}Ar-^{39}Ar dating of muscovite in an emerald-bearing quartz vein indicated 23 ± 1 million years; Sabot *et al.* 2001.)

By contrast, very little is known about the emerald deposits in Laghman Province (Laurs 2001; Henn & Schmitz 2014), especially the geological setting of the gem-quality emerald occurrence near Korgun. Based on the inclusions (biotite and tremolite) and chemical composition (rich in alkalis and alkaline earths), these emeralds appear to have a distinctly different formation environment than those of the Panjshir Valley. Due to their similar properties and trace-element content compared to emeralds from Zambia (Kafubu) and Ethiopia (Shakiso), we speculate that their formation might be similarly linked to metabasites that were metasomatically altered by Be-bearing fluids from

nearby granitoid intrusions. To our knowledge, the emerald occurrence near Korgun has produced only a limited amount of gem-quality emeralds (Laurs 2001), which are only rarely encountered in the gem trade.

For a more detailed description of the geology of emerald deposits in Afghanistan, readers are referred to Groat *et al.* (2014), Giuliani *et al.* (2019) and references therein.

MATERIALS & METHODS

We analysed 113 emeralds from Afghanistan (summarised in Table I), ranging from 0.12 to 21.22 ct: 51 showing properties consistent with Panjshir type I, 54 Panjshir type II and eight from Laghman Province (hereafter referred to as 'Laghman type' and assumed to be from the Korgun locality). Most were faceted stones (e.g. Figure 3), with only a few crystal fragments, and all of the Panjshir samples were of fine gem quality, showing good to excellent clarity and a well-saturated green colour. A detailed list of all samples is available in *The Journal*'s online data depository at https://gem-a.com/the-journal-of-gemmology-data-depository.

All samples were meticulously investigated with a microscope (System Eickhorst Gemmaster, 10–70× magnification) and analysed by standard gemmological methods, including RI, hydrostatic SG and UV fluorescence (254 and 365 nm). Ultraviolet-visible-near infrared (UV-Vis-NIR) absorption spectra (polarised o-ray) of all samples were recorded with either: (1) an Agilent Cary 5000 instrument in absorption mode (normalised path length) at 290–900 nm, with a step size of 0.35 nm and a scan rate of 0.5 s per step; or (2) our in-house-developed portable UV-Vis-NIR spectrometer equipped with an Avantes high-resolution spectrometer and using a xenon flash and halogen lamp as excitation sources.

Raman micro-spectroscopy of selected emeralds and their inclusions was performed using a Renishaw inVia spectrometer attached to a Leica DM2500 M microscope.

The system utilised an argon-ion laser (514.5 nm) and had a spectral resolution of 1.5 cm^{-1}. All analyses were carried out in confocal mode using a 20× objective to focus on the surface or within the samples (for inclusions and filler identification). For the analysis of water molecule orientation in the emeralds, the *c*-axis was oriented perpendicular to the vibrational direction of the polarised Raman laser (cf. Huong *et al.* 2010). Due to the strong Cr-related fluorescence of emerald, the laser intensity had to be reduced in some cases to prevent saturation of the Peltier detector.

Polarised Fourier-transform infrared absorption spectroscopy was carried out on all samples using a Thermo Nicolet iS50 spectrometer in the 400–4000 cm^{-1} range at a resolution of 4 cm^{-1}, primarily to detect any fissure fillings (mainly oil type) that were present occasionally in these samples.

For chemical analysis we used both energy-dispersive X-ray fluorescence (EDXRF) and laser ablation inductively coupled plasma time-of-flight mass spectrometry (LA-ICP-TOF-MS) to fully characterise the trace-element contents of the emerald samples. When summarising the range of elements present, we chose the median instead of the arithmetic average, as it is more robust to outliers and thus better represents the average concentration. EDXRF analyses of 88 selected samples (40 Panjshir type I, 43 Panjshir type II and five Laghman type) were carried out under vacuum with a Thermo Scientific ARL Quant'X instrument using our in-house-developed standard procedure with six excitation energies (4, 8, 12, 16, 20 and 40 kV) for optimised sensitivity to the full range of elements detectable by this technique. For LA-ICP-TOF-MS analyses we used our GemTOF setup consisting of a 193 nm ArF excimer laser equipped with a TwoVol2 ablation chamber (NWR193UC, Elemental Scientific Lasers, USA) coupled with a commercial ICP-TOF-MS unit (*icp*TOF, Tofwerk AG, Switzerland) that was modified from an optimised ICP-Q-MS unit (iCAP Q from Thermo Fisher Scientific). On each of 55 selected

Table I: Emerald samples from Afghanistan examined for this study.

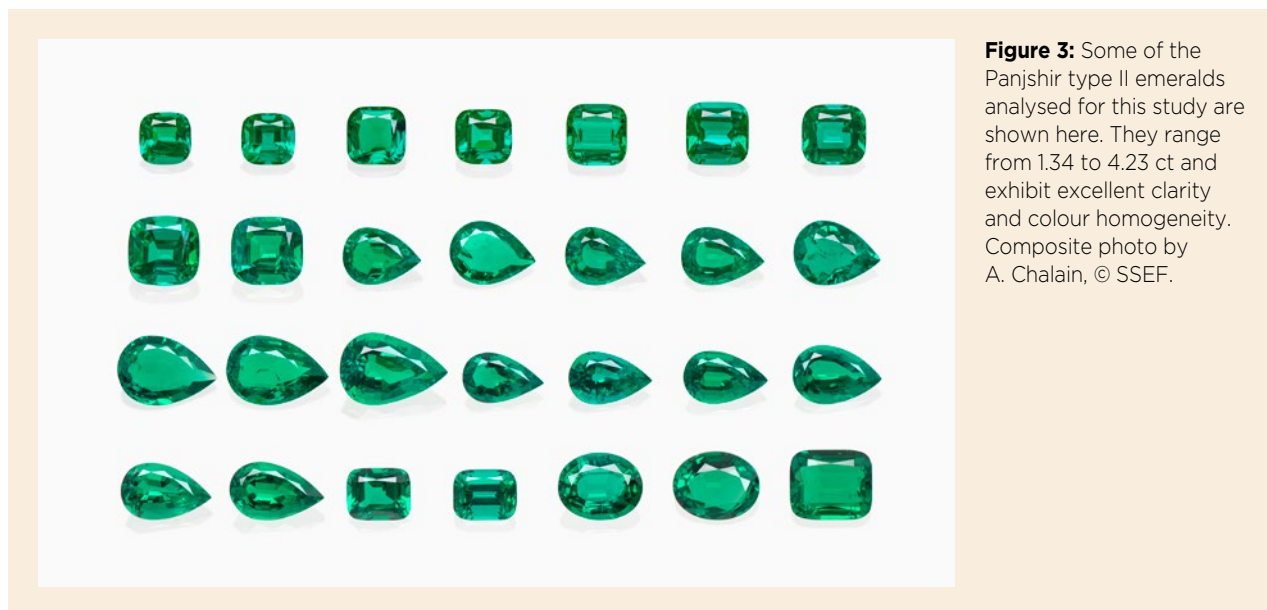| Afghan origin	Designation	Number of samples	Weight (ct)	Average SG	Average RIs	Long-wave UV fluorescence
Panjshir Valley—'classic'	Panjshir type I	51	0.43–13.79	2.74	1.581–1.589	Inert
Panjshir Valley—'new'	Panjshir type II	54	0.12–21.22	2.72	1.575–1.582	Weak to moderate red
Korgun, Laghman Province	Laghman type	8	3.17–18.58	2.74	1.580–1.588	Inert

Figure 3: Some of the Panjshir type II emeralds analysed for this study are shown here. They range from 1.34 to 4.23 ct and exhibit excellent clarity and colour homogeneity. Composite photo by A. Chalain, © SSEF.

samples (11 Panjshir type I, 36 Panjshir type II and eight Laghman type) we analysed 3–4 spots (ablation diameter 100 μm) on visually inclusion-free areas. All spots were ablated at 20 Hz and with a fluence of 5.6 J·cm⁻² using helium as the carrier gas (0.8–0.9 L/min). Five pre-cleaning laser shots were fired at the beginning of each measurement (30 s ablation time). We used NIST 610 and NIST 612 glasses as external standards, and $^{29}Si^+$ (for ideal beryl) as an internal standard.

TOF-MS (compared to more conventional quadru-pole-MS) has the advantage of simultaneous acquisition of the full mass spectrum. It allows the operator to first measure almost the entire composition of the sample and then determine which elements are of interest. This approach is ideal to detect unusual trace elements or to monitor elemental variations (e.g. due to growth zoning), or to detect and chemically charac-terise accidentally ablated (sub-microscopic) inclusions. Detailed information about instrumental parameters, analytical conditions and data processing can be found in Wang *et al.* (2016) and Wang & Krzemnicki (2021).

For data interpretation and discussion, the analysed elemental concentrations were plotted in two-dimen-sional (2D) and three-dimensional (3D) diagrams, combining our analyses for the investigated Afghan emeralds with SSEF's reference database for emerald samples from other origins (92 from Colombia, 26 from Ethiopia, two from Nigeria, 23 from Pakistan and 104 from Zambia). We further evaluated the chemical data using t-distributed stochastic neighbour embedding (t-SNE), a statistical method for dimension reduction. This machine-learning algorithm has proven to be a versatile method for the non-linear transformation of high-dimensional datasets (e.g. multi-element concentrations from mass spectrometry) into a low-dimensional space (van der Maaten & Hinton 2008). The unsupervised algorithm used by this technique means that the data input into the statistical calculation are not labelled with their origin *a priori*. The t-SNE scatter points are colour-coded according to their respective origins only after t-SNE analysis, and the clustering or grouping of data points is purely due to their elemental similarity. This method allows us to better visualise sample relationships and place separate mineral data sets into various subgroups. A detailed description of this statistical methodology for an emerald case study is provided in Wang & Krzemnicki (2021). In the present study, we calculated the t-SNE plot using concentrations of 56 elements from more than 1,100 spot analyses of 360 emerald samples. A list of the 56 elements used for this process is provided in the data depository.

RESULTS

The analysed Panjshir type II emeralds were mostly of excellent quality (e.g. Figure 3), with few fissures and a homogeneous and well-saturated green colour, reminiscent of the best-quality Colombian emeralds. As such, these stones can be considered mostly superior to the average quality of Panjshir type I emeralds and definitely more attractive than the rather included and moderately saturated Laghman-type emeralds.

Standard gemmological testing revealed rather low RI (1.575–1.582) and SG (2.72) values for the Panjshir type II material, similar to Colombian emeralds, and distinctly lower values than those of Panjshir type I and

Laghman-type emeralds (see Table I). In addition, only the Panjshir type II emeralds showed a reddish fluorescent reaction to long-wave UV radiation, whereas all the studied Panjshir type I and Laghman-type emeralds were inert (consistent with their distinctly higher Fe concentrations; see below).

Internal Features

Careful and meticulous microscopic observation is the basis for robust gemmological research and expertise—particularly when studying material from different origins or mines—as was the case for the three different types of Afghan emeralds examined in this study. Surprisingly, there are few detailed published descriptions of microscopic features in Panjshir emeralds (Bowersox *et al.* 1991; Schwarz & Pardieu 2009). Table II summarises the microscopic characteristics reported in the literature alongside those we observed in our Panjshir type I, Panjshir type II and Laghman-type samples.

In Panjshir type I emeralds (Figure 4a), spiky-to-tubular

Table II: Inclusion features in the Afghan emeralds.[a]

Feature	Panjshir type I	Panjshir type II	Laghman type
General appearance	Mostly included	Often rather clean	Often highly included
Colour zoning	Occasional hexagonal colour zoning	—	Occasional colourless hexagonal zones
Growth structures	Dense growth lines || to *c*-axis	Dense growth lines || to *c*-axis; occasional swirled to chevron-like structures	Dense growth lines || to *c*-axis
Main fluid inclusions	Spiky and tubular multiphase	Small, spiky to tubular and 'sawtooth' multiphase	Small, irregular to slightly rectangular two-phase and multiphase
Hollow channels || to *c*-axis	Coarse to fine, partly filled with FeO(OH)	Fine and often densely arranged; partly kinked or slightly curved	Coarse, partly filled with graphite
Etch tubes	Coarse, often filled with FeO(OH)	Fine, irregular to curved; partially filled with FeO(OH)	—
Platelets/cavities	—	Occasional flat, semicircular surface cavities partially filled with FeO(OH)	Numerous tiny platelets ⊥ to *c*-axis
Fine particles	Not common	—	Dispersed in zones or in 'dust' lines
Solid inclusions:			
Feldspar (microcline and albite)	Occasional	Rare	—
Quartz[b]	Occasional	—	—
Phlogopite	—	—	Very common
Tremolite	—	—	Very common
Tourmaline[b]	Occasional	—	—
Dolomite	Occasional	—	—
Rhombic carbonate (ankerite)[b]	Occasional	—	—
Apatite	—	Rare	—
Phosphate (monazite/eosphorite)[b]	Rare	—	—
Rutile	Rare	Rare	—
Pyrite	Rare	—	—

[a] Abbreviations: — = not observed, \|\| = parallel and ⊥ = perpendicular.
[b] From the literature: Bowersox *et al.* (1991), Schwarz and Pardieu (2009), and Henn and Schmitz (2014).

(along the *c*-axis) halite-sylvite-bearing multiphase fluid inclusions are typically seen (Giuliani *et al.* 2018; see Figures 4b and 4c). Occasionally we observed distinct hexagonal colour zoning—with a lighter core and a darker green rim—when looking along the *c*-axis (Figure 4d), and in some cases dense growth lines parallel to the *c*-axis. Other common features were fine (Figure 4e, f) to rather coarse (Figure 4g, h) hollow tubes parallel to the *c*-axis, which were often partially filled with brownish

Fe-hydroxide (identified by Raman micro-spectroscopy) and some black foreign substance (presumably residue of the cutting process). Fe-hydroxide was commonly present in the fissures and cavities of most of the Panjshir type I emeralds (cf. Bowersox *et al.* 1991), as also observed on the outer surface of one crystal (Figure 4i). In our samples we found only a few solid inclusions, among them octahedral pyrite, rhombic dolomite, rutile and small grains of microcline (K-feldspar), which were
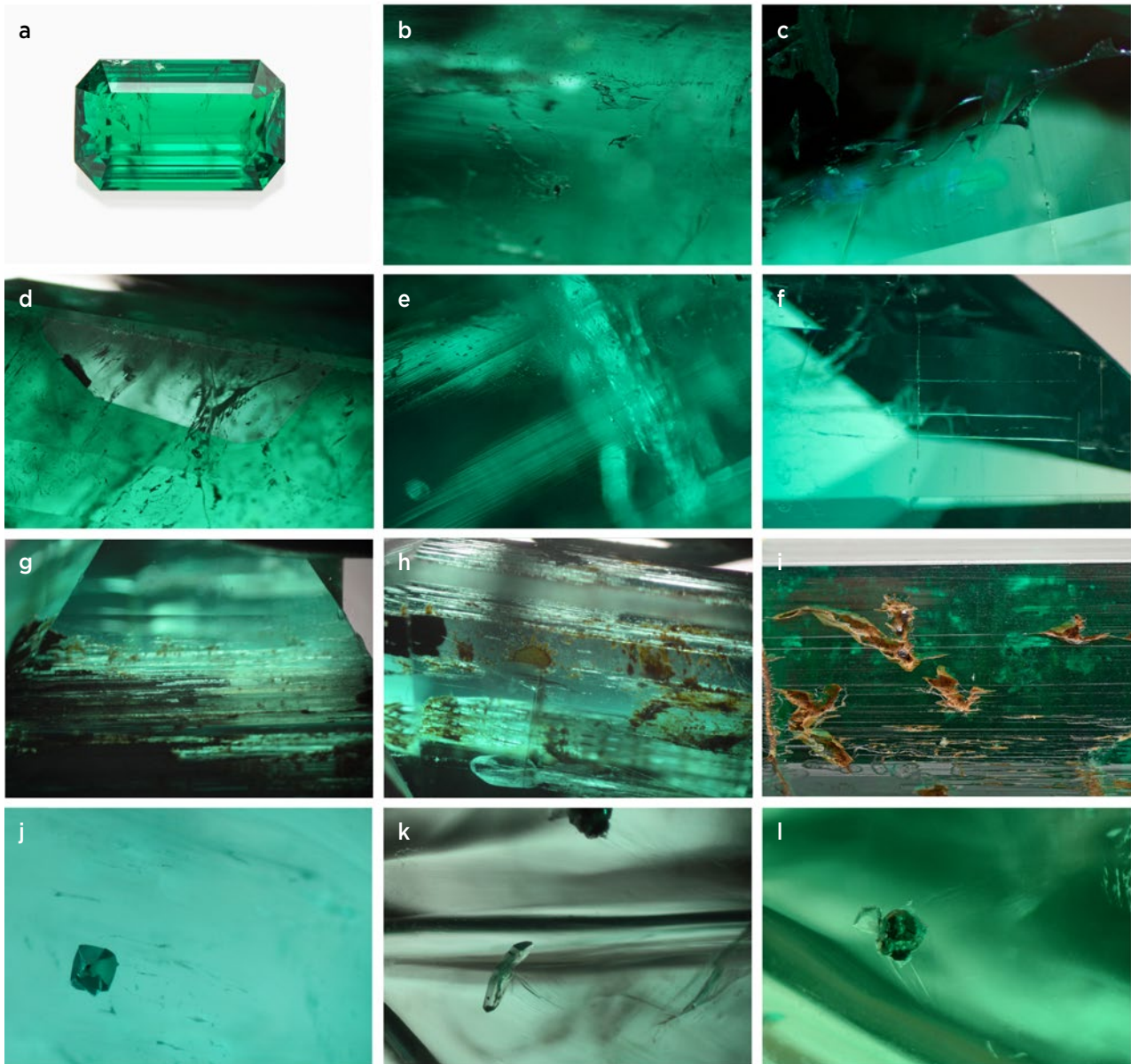

Figure 4: (**a**) This fine-quality 4.82 ct Panjshir type I emerald is typical of the material in which the inclusions shown here were observed. Features seen in Panjshir type I emeralds include: (**b**) and (**c**) spiky and tubular (along the *c*-axis) halite-sylvite-bearing multiphase fluid inclusions (both magnified 50×); (**d**) hexagonal colour zoning seen looking down the *c*-axis (magnified 30×); (**e**) fine and dense growth lines parallel to the *c*-axis (magnified 40×); (**f**) fine hollow channels parallel to the *c*-axis (magnified 30×); (**g**) a dense pattern of coarse hollow tubes oriented along the *c*-axis, partially filled with Fe-hydroxide and a black foreign substance, presumably residue from the cutting process (magnified 20×); (**h**) coarse hollow channels filled with brownish aggregates of Fe-hydroxide (magnified 20×); (**i**) etch features lined with Fe-hydroxide on the surface of an emerald crystal (magnified 10×); (**j**) a pyrite octahedron (magnified 70×); (**k**) a flat rhombic dolomite crystal (magnified 50×); and (**l**) microcline accompanied by pyrite (magnified 70×). Photomicrographs by M. S. Krzemnicki, © SSEF.

all identified by Raman micro-spectroscopy (Figures 4j–l). Other inclusions—such as ankerite, tourmaline and a phosphate—have been mentioned in the literature (Bowersox *et al.* 1991; Schwarz & Pardieu 2009) but were not observed in our samples.

The internal features in the Panjshir type II emeralds showed some resemblance to those in the type I stones, but we also observed notable differences. The most intriguing characteristic was fewer inclusions overall, resulting in a number of fine-quality eye-clean stones

(e.g. Figure 5a). Occasionally, the Panjshir type II emeralds showed fine growth features such as zones of swirly structures (Figure 5b) or chevron-like shapes (Figure 5c), and occasionally dense growth lines parallel to the *c*-axis. However, we did not observe the columnar honeycomb pattern (also known as *gota de aceite*) that is seen in some Colombian emeralds. Some irregular-to-curved etch channels were present (Figure 5d), often filled partially with Fe-hydroxide. In some cases, flat semicircular cavities occurred at the surface
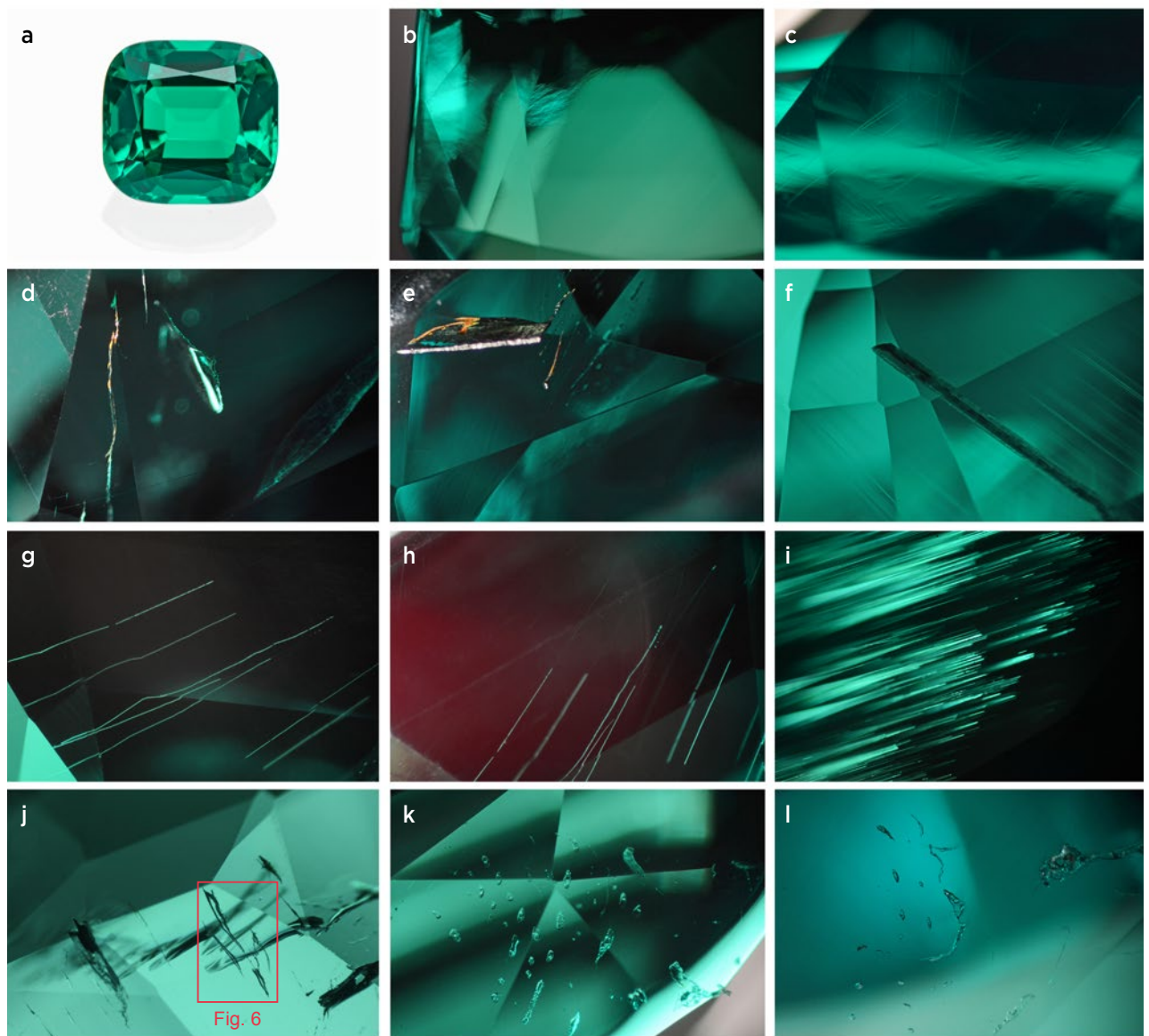

Figure 5: (**a**) A 2.42 ct Panjshir type II emerald displays the excellent quality of some of this relatively new material from Afghanistan. Inclusions in such Panjshir type II emeralds can consist of: (**b**) occasional fine, swirly to (**c**) chevron-like growth zoning (both magnified 50×); (**d**) irregular-to-curved, fine etch channels partially filled with Fe-hydroxide (magnified 60×); (**e**) a flat semicircular cavity at the surface, along with etch channels partially filled with Fe-hydroxide (magnified 50×); (**f**) a flat hollow channel parallel to the *c*-axis filled with epigenetic material (magnified 30×); (**g**) a few slightly irregular and kinked hollow channels parallel to the *c*-axis (magnified 50×); (**h**) reddish visible fluorescence together with a few hollow channels (magnified 50×); (**i**) a dense pattern of fine hollow channels parallel to the *c*-axis (magnified 50×); (**j**) tubular multiphase fluid inclusions with 'sawtooth' outlines (magnified 30×); (**k**) a group of irregularly shaped multiphase fluid inclusions (magnified 30×); and (**l**) tiny spiky multiphase fluid inclusions (magnified 70×). Photomicrographs by M. S. Krzemnicki, © SSEF.

(Figure 5e), presumably relict of a dissolved primary phase (possibly tabular calcite crystals). Solid inclusions were rather rarely observed and consistently very small in the Panjshir type II samples. These consisted of albite, rutile and a tiny prismatic apatite crystal (all identified by Raman micro-spectroscopy).

Also, like Panjshir type I emeralds, the type II stones additionally contained both hollow channels along the *c*-axis (e.g. Figure 5f) and spiky-to-tubular multiphase fluid inclusions (Krzemnicki 2018). However, the hollow channels were mostly very thin and slightly curved or locally bent, and usually did not contain Fe-hydroxide (Figures 5g and 5h). These hollow channels were the dominant inclusion feature in some samples (Figure 5i), and were much more apparent than in Colombian emeralds, where similar channels are even thinner. The multiphase fluid inclusions in the Panjshir type II emeralds were often very small and tubular to irregular or spiky in shape (Figure 5j–l). Interestingly, some of these primary fluid inclusions showed a distinct 'sawtooth' outline (Figures 5j–k and 6; see also Hughes 2021), which in our opinion is unique to Panjshir type II material.

The Laghman-type emeralds showed very different inclusion features and therefore cannot be misinterpreted as Panjshir emeralds. They tended to be quite included and often showed rather low colour saturation (Figure 7a; see also Henn & Schmitz 2014), at least compared to Panjshir emeralds. All of our Laghman-type
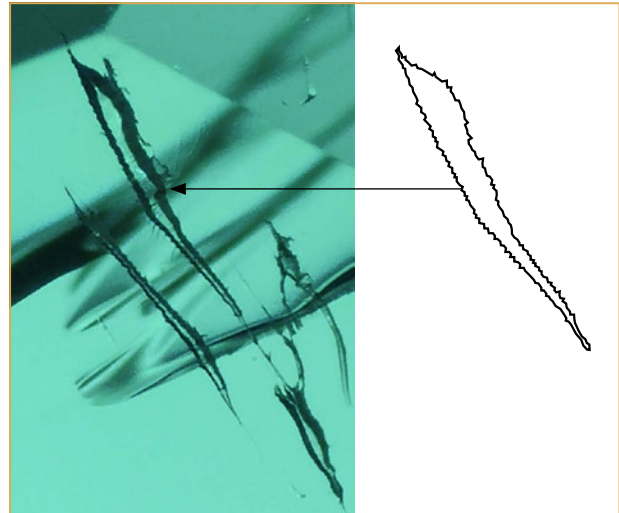

Figure 6: Tubular fluid inclusions with a distinct sawtooth outline were observed in Panjshir type II emeralds. Photo by M. S. Krzemnicki, © SSEF; magnified 70×.

samples were characterised by the presence of tremolite (Figure 7b), often as randomly oriented, slightly curved needles (Figure 7c). In addition, they all contained numerous slightly brownish phlogopite flakes (Figure 7d). Both tremolite and phlogopite were identified by Raman micro-spectroscopy. The Laghman-type emeralds also contained two-phase fluid inclusions with irregular to slightly rectangular shapes (Figure 7e), as well as fine platelets dispersed in zones or aligned as 'dust
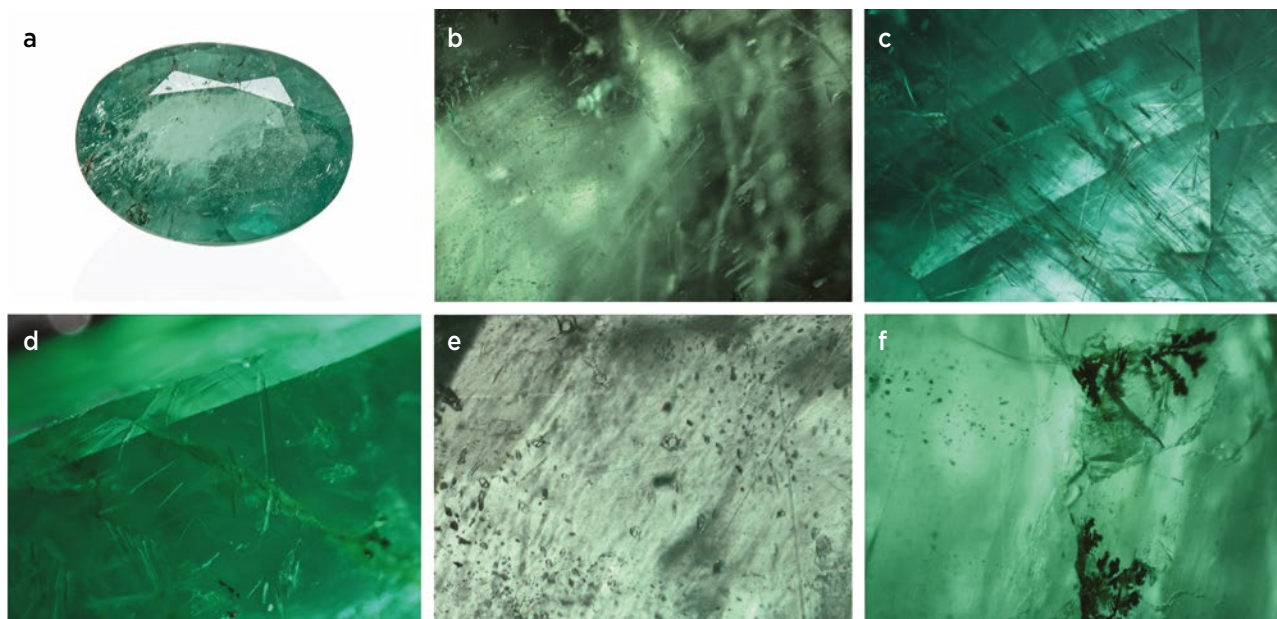

Figure 7: (**a**) A typical 3.17 ct Laghman-type emerald shows the generally included appearance and lower colour saturation of this material. Typical internal features in Laghman-type emeralds include: (**b**) near-colourless tremolite needles (magnified 40×); (**c**) dense patterns of randomly oriented and slightly curved tremolite needles (magnified 30×); (**d**) many slightly brownish flakes of phlogopite (magnified 40×); (**e**) tiny irregular to slightly rectangular two-phase fluid inclusions (magnified 50×); and (**f**) fissures containing graphite dendrites (magnified 50×). Photomicrographs by M. S. Krzemnicki, © SSEF.

lines'. Open fissures and cavities were often filled with secondary black dendritic material (Figure 7f), which was identified by Raman analysis as graphite (of rather low crystallinity).

UV-Vis-NIR Spectroscopy

The green colour of emerald is well known to be linked not to the presence of Cr alone, but to a complex interplay of the transition metals Cr, V and Fe in the beryl structure (Wood & Nassau 1968), and this was also shown by the Afghan emeralds in this study. Their UV-Vis-NIR spectra (for the ordinary ray, equivalent to E⊥c) could be separated into two groups: (1) Panjshir type I and Panjshir type II, and (2) Laghman type (Figure 8).

The spectra of the Panjshir emeralds were mostly dominated by broad absorption bands centred at approximately 435 and 605 nm due to octahedrally coordinated Cr^{3+} and V^{3+}, and by small, sharp, spin-forbidden Cr bands in the 600–700 nm range (Wood & Nassau 1968; Schmetzer 2014 and references therein). In the Panjshir type I emeralds, the band at approximately 435 nm was occasionally superimposed by a shoulder at about 390 nm attributed to V^{3+} at the octahedrally coordinated Al^{3+} site of the beryl structure (Schmetzer et al. 2006), consistent with the considerable V concentrations in those samples. In addition, a small feature at about 375 nm related to octahedrally coordinated Fe^{3+} was occasionally present. A common feature of all Panjshir
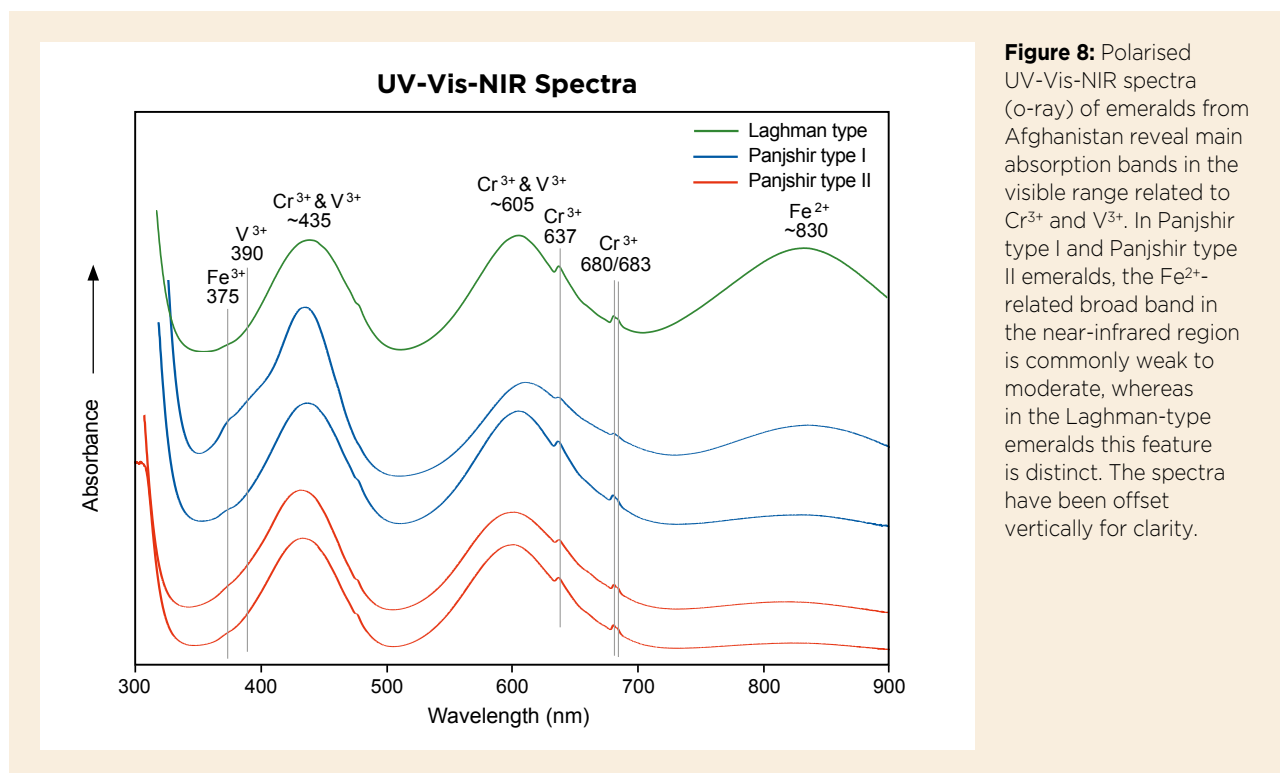
emeralds is a broad absorption band in the near-infrared region at about 830 nm, which is related to octahedrally coordinated Fe^{2+} (Wood & Nassau 1968; Taran & Rossman 2001). The intensity of this band can vary from very weak to moderate in Panjshir emeralds. By contrast, the spectra of the relatively Fe-rich Laghman-type emeralds were distinctive in showing a significantly stronger Fe^{2+} absorption band at about 830 nm; this is among the features that are sometimes described as the 'aquamarine component' in such Fe-rich emeralds.

Raman Spectroscopy: Type I and Type II H₂O

Raman micro-spectroscopy was used to determine the average orientation of H_2O molecules in the beryl channel structure (cf. Huong 2008; Huong et al. 2010), based on the relative intensity of the bands at 3608 cm^{-1} (type I H_2O) and 3598 cm^{-1} (type II H_2O). Interestingly, the three types of Afghan emeralds in this study revealed distinct differences in the patterns of these bands (Figure 9).

For the Panjshir type II emeralds, type I H_2O clearly dominated over type II H_2O, indicating that the axis of the water molecules in these emeralds is predominately perpendicular to the c-axis (and channel axis; see Wood & Nassau 1968; Huong et al. 2010). This is consistent with their low concentration of alkali elements, as determined by the chemical analyses (see below).

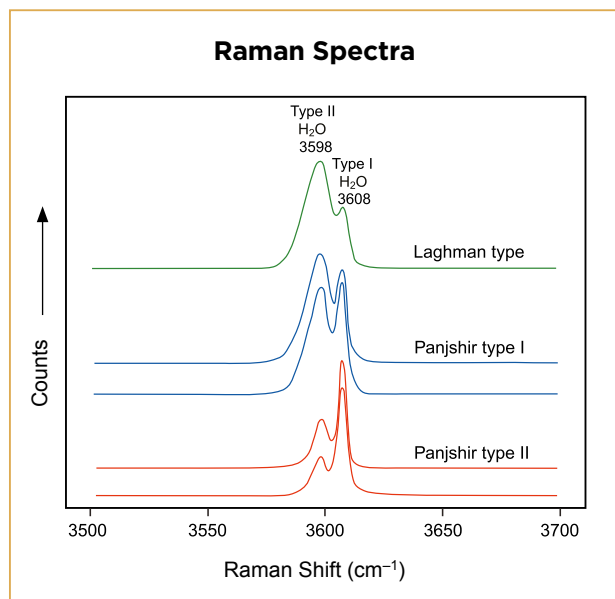By contrast, the Panjshir type I emeralds generally

Figure 8: Polarised UV-Vis-NIR spectra (o-ray) of emeralds from Afghanistan reveal main absorption bands in the visible range related to Cr^{3+} and V^{3+}. In Panjshir type I and Panjshir type II emeralds, the Fe^{2+}-related broad band in the near-infrared region is commonly weak to moderate, whereas in the Laghman-type emeralds this feature is distinct. The spectra have been offset vertically for clarity.

Raman Spectra

Type II
H₂O
3598

Type I
H₂O
3608

Laghman type

Panjshir type I

Panjshir type II

Counts

3500 3550 3600 3650 3700

Raman Shift (cm⁻¹)

Figure 9: Raman spectra show variable band intensities corresponding to the different orientations of the water molecules in the channel structure (i.e. type I and type II H₂O; after Huong *et al.* 2010) for emeralds from the three studied occurrences in Afghanistan. The spectra have been offset vertically for clarity.

parallel to the *c*-axis. This is characteristic of emeralds hosted in mafic to ultramafic host rocks (i.e. deposit types IA and IIA; Giuliani *et al.* 2019), which typically contain notable amounts of alkali elements (Na, K, Rb and Cs) in the channels of the beryl structure.

EDXRF Chemical Analysis

EDXRF spectroscopy is for many gem laboratories the standard method to obtain chemical data from gems, and this technique can sometimes provide important information about the origin and geological context of a sample—particularly for emeralds, with their extensive possibilities for chemical substitutions in the different lattice sites and the channel structure of beryl (Groat *et al.* 2014). Table III summarises the results for selected elements as determined by EDXRF spectroscopy for the Afghan emeralds and for samples from SSEF's reference collection. As with the water-related Raman spectra described above, the trace-element compositions of the three types of emeralds were quite distinct from each other.

Although the Mg concentrations in our samples varied considerably, the Panjshir type I and Laghman-type emeralds generally contained distinct amounts of this element (Panjshir type I median = 0.70 wt.% MgO and Laghman-type median = 1.41 wt.% MgO). By contrast, Mg was not detectable in any of the Panjshir type II emeralds with our EDXRF spectrometer.

The average concentrations of the chromophores V, Cr and Fe also showed distinct trends for all three types

showed essentially equal intensities of both H₂O bands, thus indicating no particular abundance of the water-molecule orientation parallel or perpendicular to the *c*-axis.

Interestingly, the Laghman-type emeralds were distinct from both types of Panjshir emeralds by the predominance of type II H₂O. This indicates that the axis of most water molecules in these emeralds is oriented

Table III: Chemical composition by EDXRF of the Afghan emeralds compared to those from other sources.*

Oxides (wt.%)	Panjshir type I (40 samples)	Panjshir type II (43 samples)	Laghman type (5 samples)	Muzo, Colombia	Muzo, Colombia (high Sc)	Kafubu, Zambia
MgO	0.11–1.76 (0.70)	bdl	0.84–1.92 (1.41)	bdl	bdl	1.98
Sc₂O₃	0.04–0.64 (0.31)	bdl–0.14 (0.04)	0.02–0.06 (0.02)	0.04	0.35	bdl
V₂O₃	0.10–1.61 (0.93)	0.15–0.42 (0.31)	0.02–0.05 (0.03)	0.83	0.73	0.04
Cr₂O₃	0.16–0.72 (0.31)	0.32–0.86 (0.54)	0.41–0.85 (0.69)	0.64	0.10	0.43
Fe₂O₃	0.47–2.84 (0.89)	0.20–0.42 (0.28)	0.43–0.67 (0.48)	0.10	0.13	2.86
Cs₂O	bdl	bdl	0.08–0.13 (0.10)	bdl	bdl	0.14

* Numbers in parentheses are median values. Representative analyses of Colombian and Zambian emeralds were selected from SSEF's database. Abbreviation: bdl = below detection limit (commonly 0.002 wt.% for heavy elements and 0.1–0.5 wt.% for light elements).
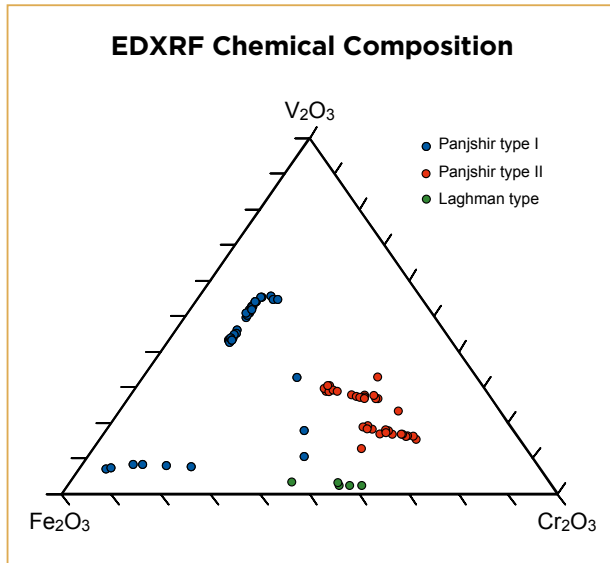
Figure 10: EDXRF chemical data for the chromophores V, Cr and Fe are plotted in this ternary diagram (after Graham & Midgley 2000) for the three different emerald types from Afghanistan.

of Afghan emeralds (Figure 10). Panjshir type I emeralds generally had the greatest amount of V (up to 1.61 wt.% V_2O_3). The V-rich emeralds also commonly showed the highest Sc concentrations (up to 0.64 wt.% Sc_2O_3) of all the samples we tested, indicating a positive correlation trend for V and Sc in Panjshir emeralds.

In general, the Cr concentration of our Panjshir type I emeralds was lower (median 0.31 wt.% Cr_2O_3) than the amount of Fe (median 0.89 wt.% Fe_2O_3). By contrast, the Cr concentration of the Panjshir type II emeralds (up to 0.86 wt.% Cr_2O_3) was distinctly higher than Fe (median of only 0.28 wt.% Fe_2O_3), with V values equal to or lower than those of Cr.

The Laghman-type emeralds were very poor in V and Sc but contained appreciable amounts of Cr (median = 0.69 wt.% Cr_2O_3) and Fe (median = 0.48 wt.% Fe_2O_3). The alkali metal Cs (residing in the beryl channel structure) was detected by EDXRF only in the Laghman-type emeralds (see also Henn & Schmitz 2014).

Comparing our Afghan emeralds with selected samples from other important sources, the chemical composition of the Laghman-type samples was consistent with those from schist-hosted deposits (i.e. types IA and IIA after Giuliani *et al.* 2019), such as Kafubu, Zambia. The Panjshir type II material was similar in composition to emeralds from Colombia (including those with high Sc; again, see Table III).

LA-ICP-TOF-MS Chemical Analysis

Table IV summarises the results of LA-ICP-TOF-MS analyses of our Afghan emerald samples. The data

show that, similar to our EDXRF results, the three types of Afghan emeralds can be conclusively distinguished by their trace-element compositions. However, mass spectrometry is sensitive to a much larger range of elements, so it provides data not accessible by EDXRF, specifically regarding light elements (e.g. Li, Be and B) and ultra-trace elements (in this case, Ge, Sr and Tl).

The Laghman-type emeralds generally contained more chemical impurities than the Panjshir emeralds. Specifically, they showed distinctly higher concentrations of Li, B, Mn, Co, Ni, Zn, Sn, Cs and Tl. The distribution of chromophores (V, Cr and Fe) clearly underscores the difference in the geological setting and formation of Laghman-type emeralds compared to both types of Panjshir emeralds. The Panjshir type I and Panjshir type II samples both had distinctly higher concentrations of V than the Laghman-type emeralds. In addition, some of the Panjshir type II emeralds showed distinctly higher V concentrations (up to 3105 ppm) than Panjshir type I stones—which is opposite to our EDXRF results. This might be related to chemical zoning in these emeralds, which cannot be resolved by EDXRF due to the rather large area analysed by this method. The trends in Sc concentration, however, were consistent with the EDXRF results, revealing that the highest Sc concentrations occurred in the Panjshir type I emeralds.

Plotting V vs Sc shows a distinct linear correlation, with the three types of Afghan emeralds falling into discrete groups (Figure 11a). A non-logarithmic plot (Figure 11b) reveals further correlation trends within the Panjshir type II samples.

It is well known that the incorporation of alkaline earth metals (specifically Mg^{2+} and Ca^{2+}) in the octahedrally coordinated Al^{3+} site in beryl is charge-balanced by alkali metals (specifically Na^+, K^+, Rb^+ and Cs^+) in the channel structure: $Al^{3+} \rightarrow (Mg, Ca)^{2+} + (Na, K, Rb, Cs)^+_{channel}$ (see Groat *et al.* 2014 and references therein). A plot of (Mg + Ca) vs Na (Figure 12a) shows a near-perfect positive correlation for Panjshir emeralds, in two well-discernible groups (Panjshir type I and Panjshir type II). Therefore, in these emeralds the alkaline earths (Mg and Ca) are almost completely charge balanced by Na only. By contrast, the Laghman-type emeralds are slightly offset from the r = 1 correlation line in Figure 12a. However, by taking into account all additional alkalis (K, Rb and Cs) present in the channel structure, they plot more closely to the correlation line (Figure 12b). Interestingly, in this second figure we also see that the Panjshir type I (and some type II) emeralds are slightly offset below the r = 1 correlation line, possibly indicating that some of the alkali

Table IV: Chemical composition by LA-ICP-TOF-MS of Afghan emeralds.*

Elements (ppm)	Panjshir type I (20 samples)	Panjshir type II (44 samples)	Laghman type (8 samples)
Li	81.12–212.6 (91.54)	73.36–108.7 (93.13)	216.6–371.6 (313.4)
B	bdl–1.959 (0.794)	bdl–1.171 (0.383)	2.225–5.561 (3.078)
Na	6730–11690 (9997)	3130–6210 (4141)	10920–13340 (12680)
Mg	5860–11720 (9914)	2565–5620 (3624)	12960–15050 (14300)
K	242.0–870.4 (696.2)	22.46–77.20 (33.28)	526.1–770.0 (654.6)
Ca	236.2–610.6 (385.4)	278.6–714.4 (567.8)	563.2–995.4 (829.6)
Sc	130.3–1083 (708.4)	36.83–767.3 (71.75)	36.19–111.2 (100.2)
Ti	9.87–59.91 (24.19)	4.49–17.69 (10.85)	12.51–24.20 (17.90)
V	447.6–990.7 (862.5)	595.5–3105 (824.5)	117.6–188.3 (176.3)
Cr	239.8–2979 (1223)	1878–4875 (2625)	1710–5317 (4669)
Mn	1.434–3.526 (2.212)	0.336–0.952 (0.503)	6.628–9.955 (8.128)
Fe	3963–11330 (8000)	1100–2057 (1308)	1925–2317 (2116)
Co	bdl–0.102 (0.043)	bdl–0.110 (bdl)	1.471–1.646 (1.538)
Ni	0.298–3.128 (0.644)	0.630–2.952 (1.138)	9.79–15.94 (10.88)
Zn	bdl–0.760 (0.285)	0.333–0.964 (0.627)	13.90–18.64 (15.11)
Ga	17.74–36.74 (32.14)	13.94–31.53 (17.30)	7.65–8.94 (8.06)
Ge	0.831–1.969 (1.339)	0.202–0.654 (0.295)	0.511–0.909 (0.694)
Rb	19.72–68.46 (51.92)	1.929–4.316 (2.554)	33.55–46.79 (37.78)
Sr	bdl–0.163 (bdl)	bdl–0.209 (bdl)	0.036–0.166 (0.056)
Sn	0.097–1.432 (0.349)	bdl–0.120 (0.050)	1.498–4.560 (3.827)
Cs	30.84–70.37 (45.75)	6.916–9.993 (8.725)	612.4–1334 (769.3)
Tl	0.009–0.036 (0.023)	bdl–0.014 (bdl)	0.127–0.273 (0.197)

* Numbers in parentheses are median values; bdl = below detection limit (commonly a few ppb for heavy elements to hundreds of ppb for light elements).
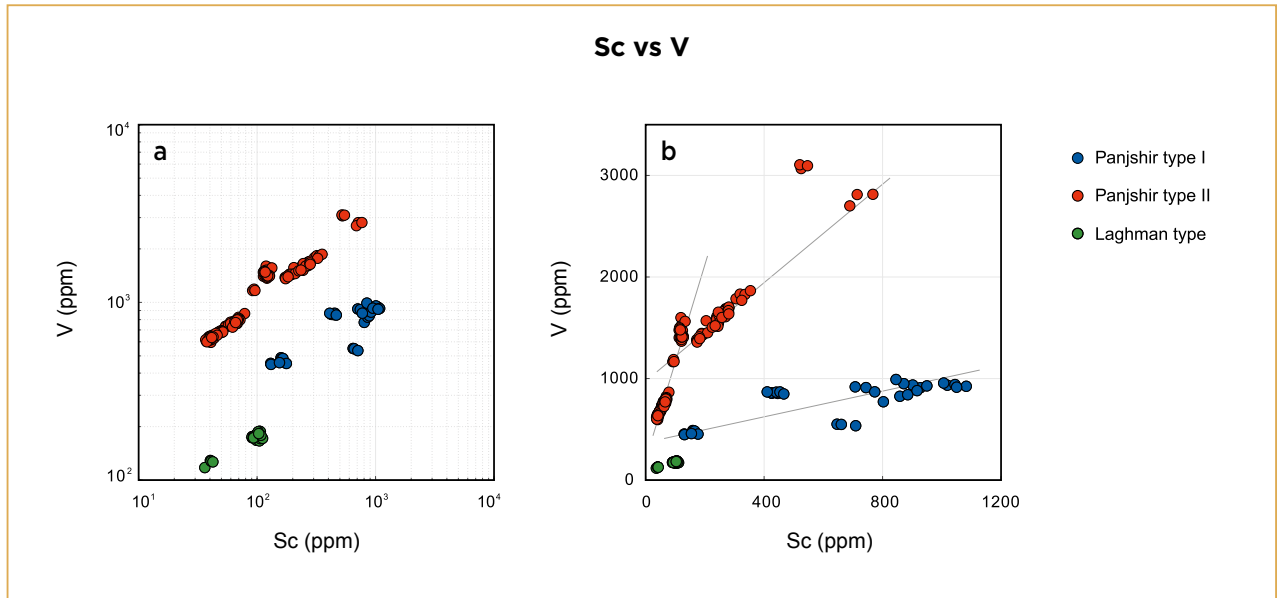
Sc vs V

Figure 11: A positive correlation between Sc and V in Afghan emeralds is shown on these scatter plots with (**a**) logarithmic axis scales and (**b**) linear axis scales. The analyses for each of the three localities also cluster into distinct groups.
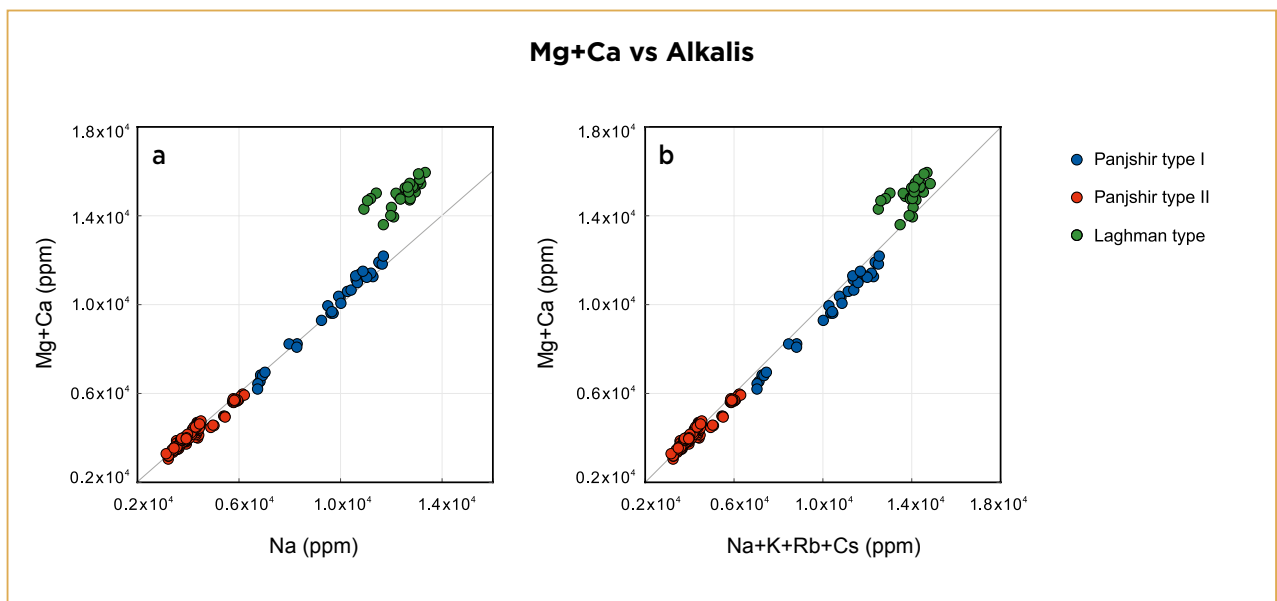
Mg+Ca vs Alkalis

Figure 12: These scatter diagrams plot octahedrally coordinated Ca + Mg vs alkali elements in the channel sites—that is, (**a**) Na and (**b**) Na + K + Rb + Cs. They reveal a distinct positive correlation—with data points falling along the r = 1 correlation line—as a result of charge-balanced substitution processes. In both diagrams, the emeralds from the three studied occurrences in Afghanistan are clearly distinct from each other along the correlation lines.

metals in the channel structure are charge-balanced by Fe^{2+} replacing Al^{3+} in the octahedral site: $Al^{3+} \rightarrow Fe^{2+} + (Na, K, Rb, Cs)^+_{channel}$. The distinct presence of Fe^{2+} in Panjshir type I emeralds was confirmed by UV-Vis-NIR spectroscopy, which revealed a weak-to-moderate broad band in the NIR attributed to octahedrally coordinated Fe^{2+} (see Figure 8).

It has been documented previously in the literature that Al substitution by alkalis and alkaline-earth metals also directly affects the physical properties of beryl,

namely SG and RI values (e.g. Winchell & Winchell 1951; Sosedko 1957; Černý & Hawthorne 1976; Hänni 1980). These correlations can also be observed in the three different types of emeralds from Afghanistan. The Panjshir type II stones, with only minor concentrations of alkalis and alkaline earths, showed the lowest SG and RI values (average SG = 2.72 and RI = 1.575–1.582), whereas the Panjshir type I and Laghman-type emeralds, with distinctly higher amounts of these elements, had greater SG and RI values (see Table I).

DISCUSSION

The three types of emeralds from Afghanistan investigated in this study can be clearly separated from each other based on their trace-element composition (as well as spectral features for Panjshir- vs Laghman-type samples). More challenging, however, is the separation of Afghan emeralds from those of other important deposits, notably from Colombia. This is specifically important for the Panjshir type II emeralds, which in many aspects are very similar to top-quality emeralds from Muzo and other famous sources in Colombia. It is therefore not surprising that a number of these Panjshir type II emeralds have been (and still are) mislabelled as Colombian stones.

Panjshir Type I vs Colombia and Davdar (China)

Panjshir type I emeralds are to some extent similar to Colombian emeralds but are still quite straightforward to identify. The spiky (jagged) halite-sylvite-bearing multiphase fluid inclusions in Panjshir type I emeralds are considered characteristic (Figure 4b, c) and help to separate them from Colombian emeralds, which contain mainly three-phase inclusions (Schwarz & Pardieu 2009; Saeseaw *et al.* 2014; Giuliani *et al.* 2018). In addition, Panjshir type I emeralds show a characteristic weak-to-moderate absorption band in the near-infrared region (Figure 13; see also Schwarz & Pardieu 2009; Karampelas *et al.* 2019), which is absent from most Colombian emeralds and only rarely encountered in some Fe-rich ones. In addition, Fe normally dominates the concentration of other colouring elements (V ± Cr) in Panjshir type I emeralds, which is distinctly different from Colombian emeralds. The visual appearance and internal features (i.e. jagged fluid inclusions) of Davdar emeralds (Schwarz & Pardieu 2009; Cui *et al.* 2020) might seem similar to Panjshir type I stones, but the Davdar emeralds can generally be distinguished by their much stronger absorption in the near-infrared region and differences in trace-element concentrations (see below).

Laghman Type (Korgun) vs Other Sources

The internal features of Laghman-type stones are similar to those found in schist-hosted emeralds related to mafic and ultramafic host rocks (i.e. types IA and IIA of Giuliani *et al.* 2019), such as from deposits in Zambia, Ethiopia and Russia, and can only be separated from those by careful examination. Their similarity is also expressed by a distinct Fe^{2+}-related absorption band in the near-infrared region (Figures 8 and 13; see also Henn & Schmitz

2014; Karampelas *et al.* 2019) and by the dominance of type II water in the beryl channel structure (more intense $3598 \ cm^{-1}$ band in Raman spectra; see Figure 9). Both of these features are highly characteristic of emeralds from deposits related to mafic and ultramafic host rocks. However, a fundamental difference is that the Laghman-type emeralds we investigated contained rather low Fe concentrations, in many cases even lower than Cr (see EDXRF data in Table III), whereas Fe is generally much higher than Cr in schist-hosted emeralds.

Panjshir Type II vs Colombia

Although Panjshir type II emeralds are challenging for origin determination, there are still various ways to make a clear and unambiguous separation from Colombian emeralds.

Meticulous microscopic observation will often reveal characteristic features of Panjshir type II emeralds, such as dense patterns of hollow channels (parallel to the *c*-axis) that are partially filled with brownish Fe-hydroxide. This is in contrast to Colombian emeralds, which sometimes show similar hollow channels, but these are extremely fine and without similar secondary
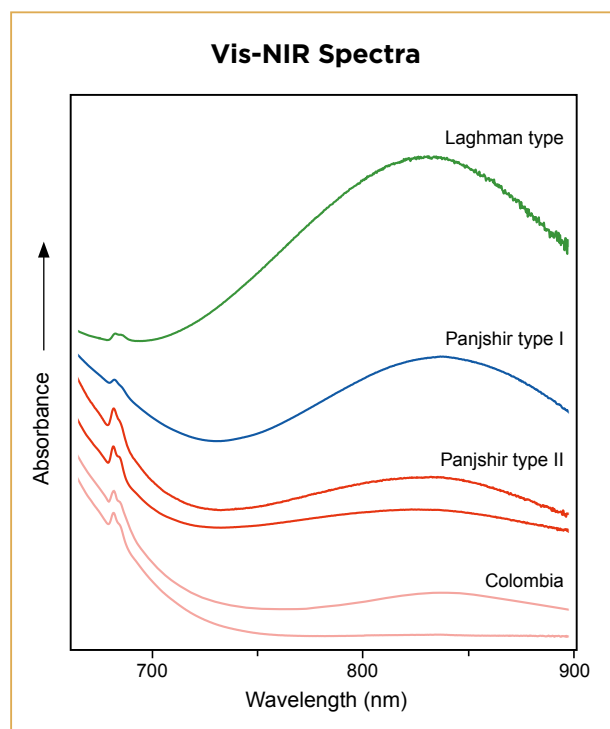

Figure 13: Polarised absorption spectra (o-ray) for the three Afghan emerald types in the red to near-infrared range show variations in the strength of the absorption band at about 830 nm, which is related to octahedrally coordinated Fe^{2+}. Panjshir type I and Panjshir type II emeralds show weak-to-moderate absorption, whereas stones from Colombia typically exhibit no such absorption feature. The spectra have been offset vertically for clarity.

Figure 14: The appearance of an unusual Fe-rich emerald from Colombia (left, 5.77 ct) that shows a weak absorption band in the near-infrared region at about 830 nm is compared to a vibrant green Panjshir type II emerald (right, 4.50 ct). Composite photo by Luc Phan, © SSEF.

natural residue. Although swirled patterns were seen occasionally in the Panjshir type II emeralds, we have not observed the distinct *gota de aceite* graining pattern seen in some Colombian emeralds.

In addition, Panjshir type II emeralds always show a weak Fe^{2+}-related absorption band at about 830 nm (Figure 13), similar to or even weaker than the Panjshir type I emeralds. This is in contrast to Colombian emeralds of high quality, which in most cases show no such absorption in the near-infrared range. Occasionally, Fe-rich Colombian emeralds may show a weak absorption in the near-infrared similar to Afghan emeralds, however those Colombian stones are usually characterised by a slightly greyish green colour of rather low saturation as compared to the vibrant green colour of Panjshir type II emeralds (Figure 14).

Raman analysis of both Panjshir type II and Colombian emeralds show a prevalence of type I H_2O (i.e. the 3608 cm^{-1}

band is clearly dominant over the 3598 cm^{-1} band), indicating a low concentration of alkali elements (Na, K, Rb and Cs) in the beryl channel structure. Therefore it is not possible to separate samples from these two origins based on this criterion.

Trace-element data provide the best option for clearly distinguishing Panjshir type II emeralds from those of Colombia. Notably, the concentration of Fe is usually distinctly higher in the Panjshir type II emeralds (Figure 15). In rare cases, gem-quality emeralds from Colombia can also show high Fe concentrations (up to 2000 ppm, according to SSEF's database, and also reported by Saeseaw *et al.* 2014 and Karampelas *et al.* 2019). However, when plotting the V/Cr ratio vs Fe, all of the Colombian emeralds in SSEF's database—including the so-called Fe-rich samples—can be clearly separated from Panjshir type II, and even more so from Panjshir type I and Laghman-type emeralds (again, see Figure 15). This was also evident from our EDXRF analyses, which showed 0.20–0.42 wt.% Fe_2O_3 in the Panjshir type II samples and generally only about 0.10 wt.% Fe_2O_3 in Colombian stones (see, e.g., Table III). In many cases, the differences between Panjshir type II and Colombian emeralds can be detected by comparing the peak ratios of V, Cr and Fe in EDXRF spectra (Figure 16). Based on this, we propose that EDXRF spectroscopy—a commonly available technique in gem labs—can be helpful for separating emeralds from these two sources. Nevertheless, this approach may not be valid for Fe-rich Colombian emeralds, and always requires further (i.e. microscopic) investigations to draw a reliable conclusion.
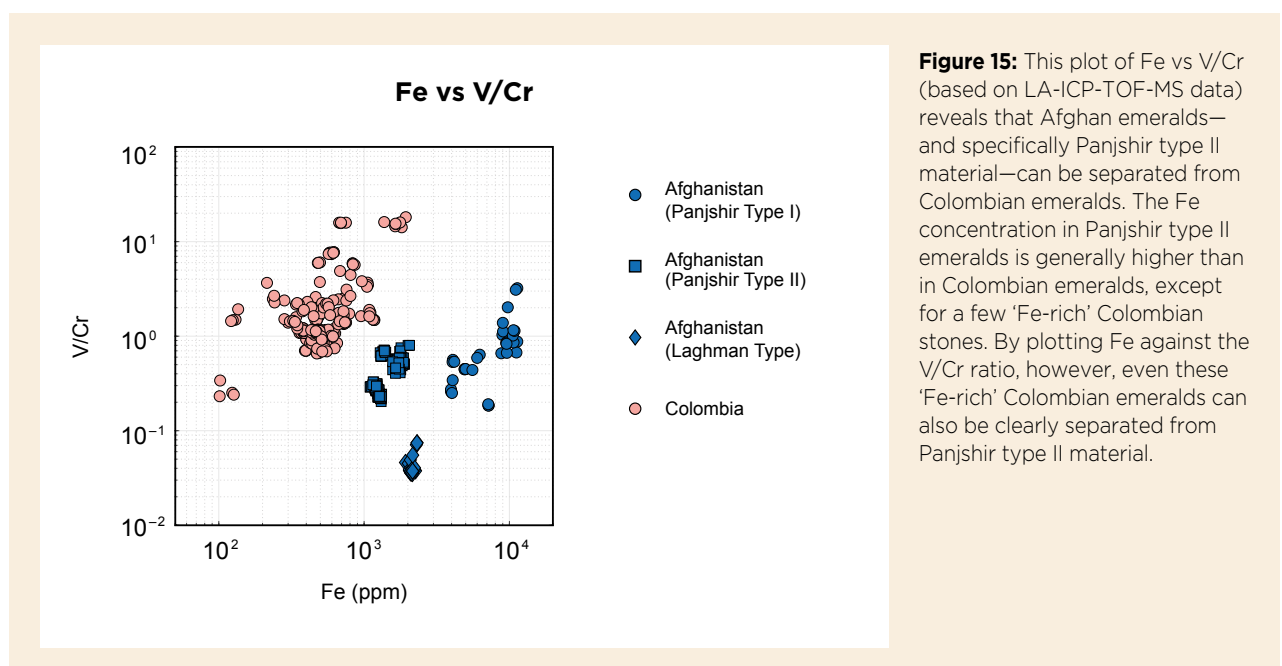

Figure 15: This plot of Fe vs V/Cr (based on LA-ICP-TOF-MS data) reveals that Afghan emeralds—and specifically Panjshir type II material—can be separated from Colombian emeralds. The Fe concentration in Panjshir type II emeralds is generally higher than in Colombian emeralds, except for a few 'Fe-rich' Colombian stones. By plotting Fe against the V/Cr ratio, however, even these 'Fe-rich' Colombian emeralds can also be clearly separated from Panjshir type II material.
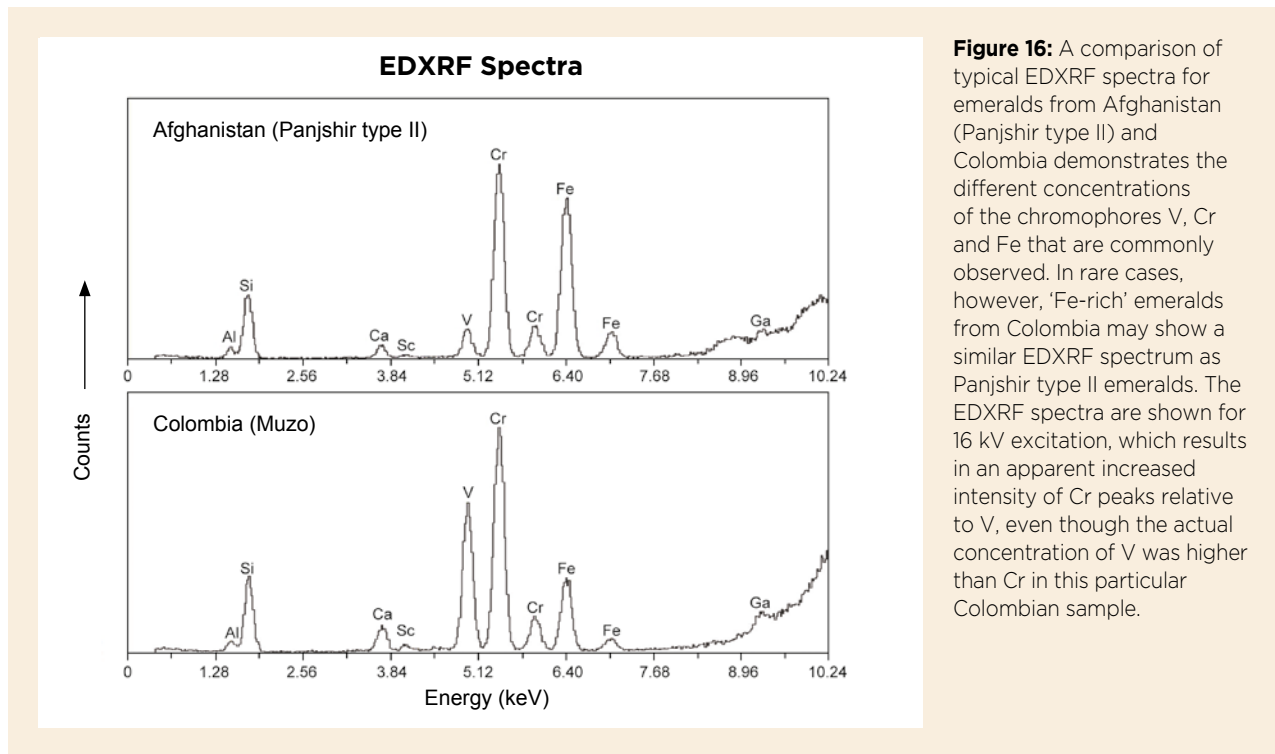
Figure 16: A comparison of typical EDXRF spectra for emeralds from Afghanistan (Panjshir type II) and Colombia demonstrates the different concentrations of the chromophores V, Cr and Fe that are commonly observed. In rare cases, however, 'Fe-rich' emeralds from Colombia may show a similar EDXRF spectrum as Panjshir type II emeralds. The EDXRF spectra are shown for 16 kV excitation, which results in an apparent increased intensity of Cr peaks relative to V, even though the actual concentration of V was higher than Cr in this particular Colombian sample.

Summary: Emeralds from Afghanistan vs Other Sources

Emeralds from different origins reveal a large chemical variability as a result of the beryl structure, which offers multiple sites for element substitutions, including a large channel structure. As such, emeralds (and beryl in general) are very susceptible indicators of the geological environment in which they formed and can be classified into different deposit/formation types (see Giuliani *et al.* 2019 and references therein).

LA-ICP-MS trace-element data can be very helpful for separating gems from different provenances (e.g. Guillong & Günther 2001; Abduriyim & Kitawaki 2006) and specifically emeralds (Cronin & Rendle 2012; Schwarz & Klemm 2012; Saeseaw *et al.* 2014; Aurisicchio *et al.* 2018; Karampelas *et al.* 2019). However, visualising trends in a large multi-element data set is often challenging and requires evaluation of multiple 2D and 3D scatter plots.

Figure 17 demonstrates how the Panjshir type I and Panjshir type II emeralds are quite similar to Colombian emeralds, whereas Laghman-type stones plot close to those from Zambia, Ethiopia and the Swat Valley in Pakistan. As seen in the Li-Cs 2D scatter plot (Figure 17a) and, even better, in the Rb-Tl-Cs 3D diagram (Figure 17d), our Panjshir type II emeralds significantly overlap Colombian emeralds, whereas in the other 2D and 3D scatter plots these data clusters are more distinct.

Emeralds from Davdar (China) are in many aspects quite similar to stones from Panjshir (Schwarz & Pardieu 2009) and even Colombian emeralds. Cui *et al.* (2020) discussed the difficulty of chemically separating Davdar emeralds from Panjshir material due to overlapping elemental concentrations. However, by plotting their data together with our LA-ICP-TOF-MS analyses, we can see a clear chemical distinction based on Ni, Rb and Cs (see Figure 18 and the rotational video clip in the data depository).

Plotting elemental ratios in a 2D diagram is another option for distinguishing emeralds from different origins based on trace elements. Figure 19 plots the ratios Cs/Ga vs Na/Li for emeralds from Colombia, Pakistan (Swat Valley), Brazil (Santa Terezinha), Austria (Habachtal), Nigeria and Russia (from Schwarz 2015 and Giuliani *et al.* 2019). Adding our data from Afghanistan and other sources (Colombia, Ethiopia, Nigeria, Pakistan and Zambia) results in significant overlaps between the various localities. Notably, the Panjshir type II emeralds plot completely within the Colombian field, and the Laghman-type emeralds overlap those from Russia and Zambia. Consequently, this ratio diagram is of only limited use for separating Afghan emeralds from those of other sources, although it is helpful for geochemical studies since it groups together emeralds of similar geological contexts.

As an alternative, we used an automated statistical algorithm (t-SNE) to visualise data clusters and sample relationships within the multi-element data set. For
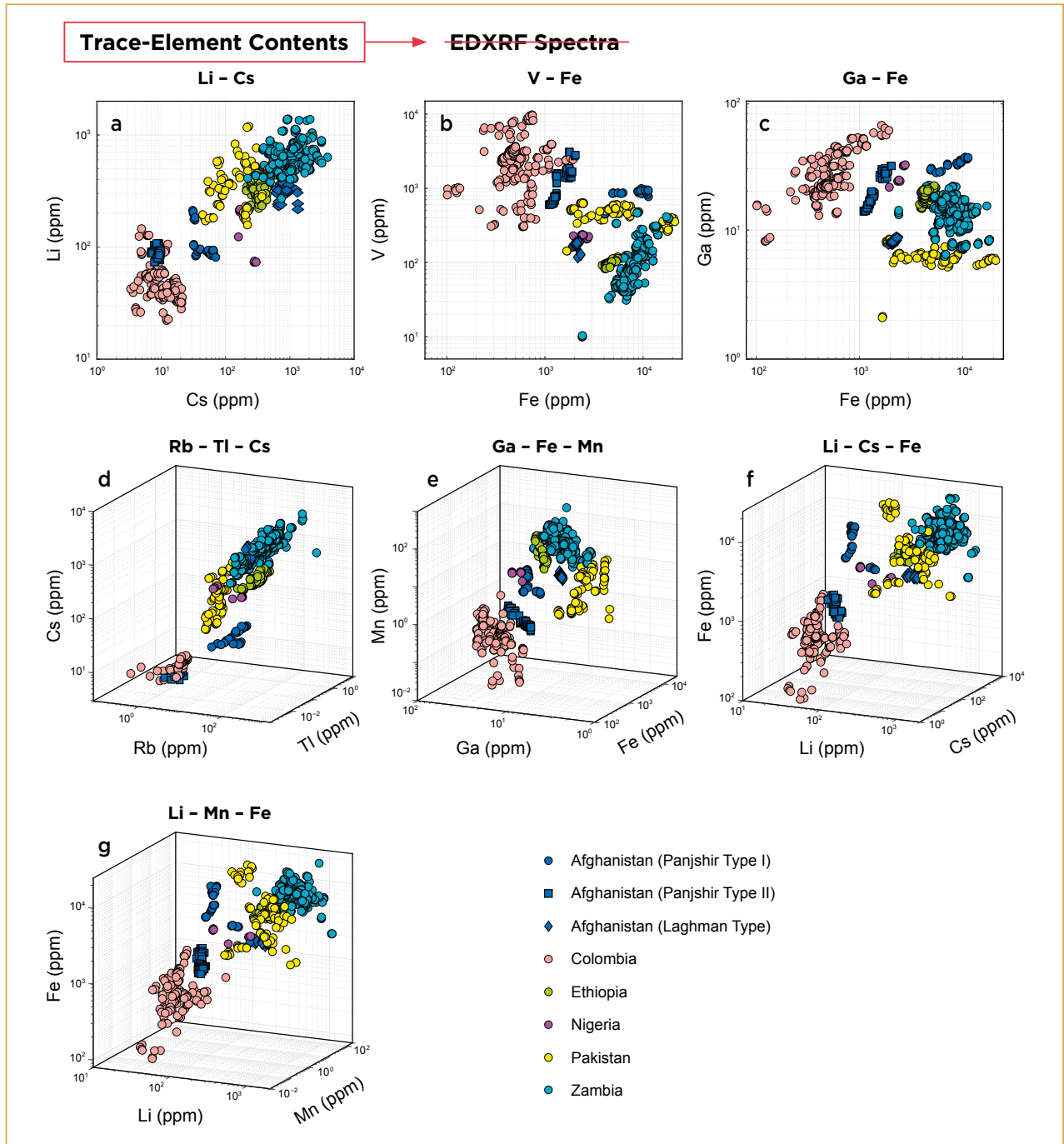
Figure 17: Scatter plots for various elements compare the three types of emeralds from Afghanistan with those from other important deposits, based on data collected at SSEF using LA-ICP-TOF-MS. Rotational video clips for each of the 3D scatter plots are available in *The Journal*'s data depository.

a detailed description of this new and versatile data processing method, see Wang and Krzemnicki (2021). The 3D t-SNE plot in Figure 20 shows that this approach is effective for distinguishing emeralds from different localities, including all three types from Afghanistan. The Panjshir type II emeralds plot in a cluster that is clearly separate from Colombian emeralds, and also from all other selected sources, including Zambia, Ethiopia, Pakistan and Nigeria. For simplicity, we have omitted from this plot some emerald deposits (mainly schist type)—such as those in Brazil (e.g. Itabira-Nova Era), Madagascar (e.g. Mananjary) and China (e.g. Yunnan)—which are easily separated from those of Afghanistan and Colombia (i.e. hydrothermal type).

For all the 3D scatter plots in Figures 17 and 20, rotational video clips are available in the data depository to better visualise the relationships between the analytical clusters for emeralds from different provenances.
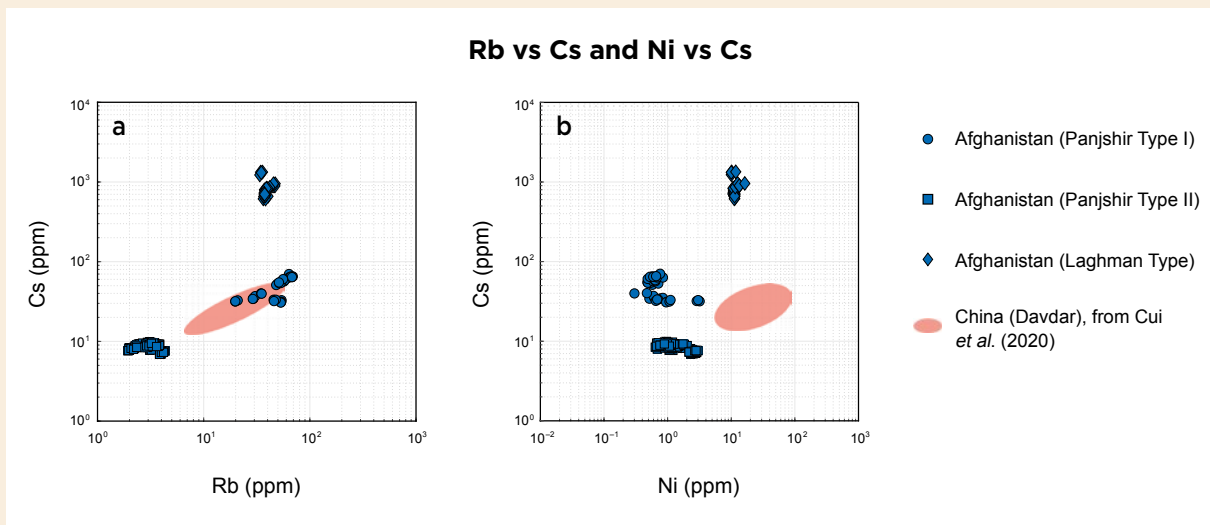
Rb vs Cs and Ni vs Cs

Figure 18: Trace-element data for Davdar emeralds (from Cui *et al.* 2020) are plotted together with analyses obtained in this study for the three types of Afghan emeralds. (**a**) A plot of Rb vs Cs shows a distinct positive correlation for both Davdar and Panjshir type I emeralds, with some overlap, whereas Panjshir type II and Laghman-type samples are clearly distinct. (**b**) A plot of Ni vs Cs clearly separates all three Afghanistan occurrences from Davdar emeralds.
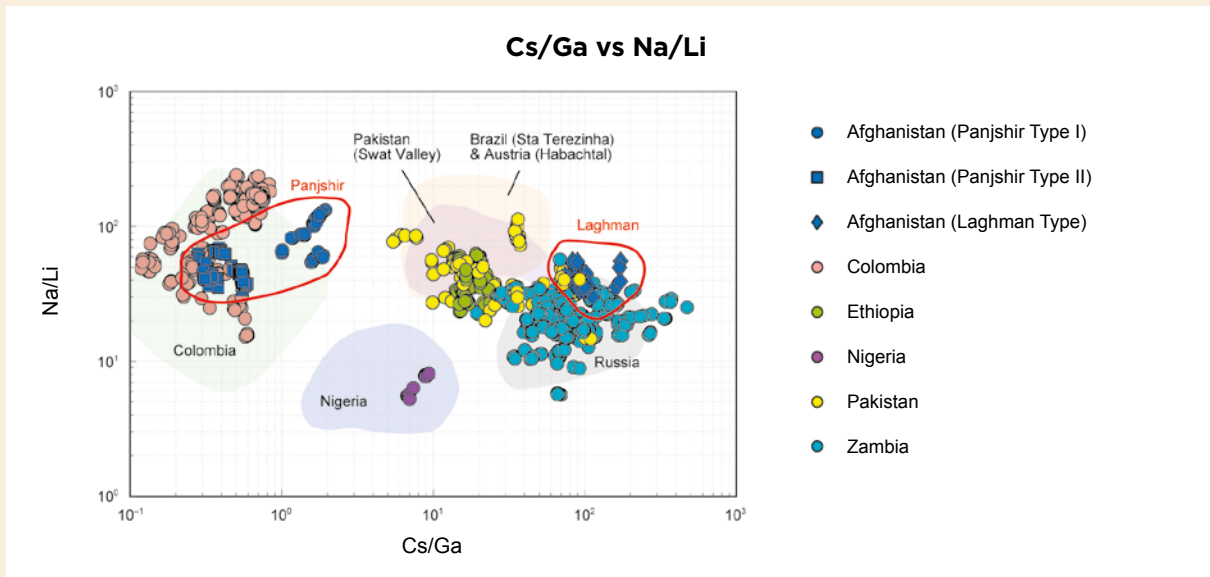
Cs/Ga vs Na/Li

t-SNE Plot

Figure 19: A plot of the ratios of Cs/Ga vs Na/Li, as proposed by Schwarz (2015) for showing genetic relationships between various types of emerald deposits, reveals that stones from Panjshir (specifically type II) and Laghman overlap with different emerald population fields. The coloured fields are from Schwarz (2015) and Giuliani *et al.* (2019).
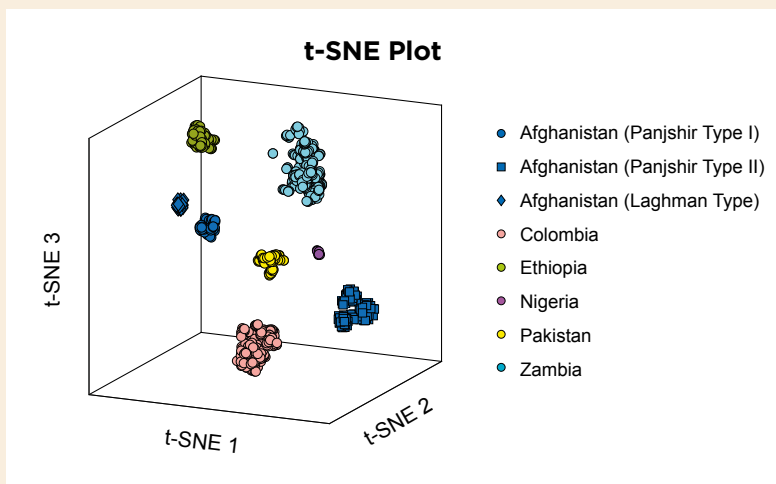
Figure 20: A 3D t-SNE scatter plot shows that data clusters for the three emerald occurrences in Afghanistan can be distinguished from each other and from other selected worldwide sources.

CONCLUSIONS

Fine-quality emeralds from Afghanistan have been known in the trade for decades, with the main source being the Panjshir Valley (providing what is referred to in this article as Panjshir type I emeralds) and a few stones coming from Laghman Province near Korgun. This study focused on relatively new emerald production from the Panjshir Valley—referred to here as Panjshir type II—which emerged on the market in 2017. This newer Afghan material is in many aspects equal to the best-quality Colombian emeralds, including some similar microscopic and chemical features. Nevertheless, we have shown that Panjshir type II emeralds can be clearly separated from their Colombian counterparts by standard gemmological techniques (e.g. microscopy) and more sophisticated analytical methods (e.g. UV-Vis-NIR, Raman and EDXRF spectroscopy, and

LA-ICP-TOF-MS). A statistical dimension-reduction algorithm (t-SNE) applied to the trace-element data from our samples provided an effective, unambiguous way to distinguish emeralds from various localities compared to typical concentration plots and element-ratio diagrams.

This study demonstrates how combining a standard gemmological approach with advanced analytical and statistical methods is useful for characterising gem materials from new sources emerging in the trade. Our research also illustrates how a new type of material can emerge from a well-known gem locality—in this case, emerald from Afghanistan's Panjshir Valley—that possesses quite different properties and trace-element concentrations as a result of local, small-scale variations in geological conditions.

REFERENCES

Abdullah, S., Chmyriov, V.M., Stazhilo-Alekseev, K.F., Dronov, V.I., Gannon, P.J., Lubemov, B.K., Kafarskiy, A.K. & Malyarov, E.P. 1977. *Mineral Resources of Afghanistan*, 2nd edn. Ministry of Mines and Industries, Afghan Geological and Mines Survey, Kabul, Afghanistan, 419 pp.

Abduriyim, A. & Kitawaki, H. 2006. Applications of laser ablation–inductively coupled plasma–mass spectrometry (LA-ICP-MS) to gemology. *Gems & Gemology*, **42**(2), 98–118, https://doi.org/10.5741/gems.42.2.98.

Aurisicchio, C., Conte, A.M., Medeghini, L., Ottolini, L. & De Vito, C. 2018. Major and trace element geochemistry of emerald from several deposits: Implications for genetic models and classification schemes. *Ore Geology Reviews*, **94**, 351–366, https://doi.org/10.1016/j.oregeorev.2018.02.001.

Bariand, P. & Poullen, J.F. 1978. Famous mineral localities: The pegmatites of Laghman, Nuristan, Afghanistan. *Mineralogical Record*, **9**(5), 301–308.

Bowersox, G.W. 1985. A status report on gemstones from Afghanistan. *Gems & Gemology*, **21**(4), 192–204, https://doi.org/10.5741/gems.21.4.192.

Bowersox, G.W. 2015. The emerald mines of the Panjshir Valley, Afghanistan. *InColor*, December, Special Issue: World Emerald Update, 70–77.

Bowersox, G., Snee, L.W., Foord, E.E. & Seal, R.R. 1991. Emeralds of the Panjshir Valley, Afghanistan. *Gems & Gemology*, **27**(1), 26–39, https://doi.org/10.5741/gems.27.1.26.

Černý, P. & Hawthorne, F.C. 1976. Refractive indices versus alkali contents in beryl: General limitations and applications to some pegmatite types. *Canadian Mineralogist*, **14**(4), 491–497.

Chmyriov, V.M., Kafarskiy, A.K., Abdullah, D., Dronov, V.I. & Stazhilo-Alekseev, K.F. 1982. Tectonic zoning of Afghanistan. *Miscellaneous Publication – Geological Survey of India*, **41**(3), 317–329.

Christie's 2015. Hong Kong Magnificent Jewels: An exceptional emerald ring. Christie's, Hong Kong, www.christies.com/lot/lot-an-exceptional-emerald-ring-5952358, accessed December 2020.

Cronin, D.P. & Rendle, A.M. 2012. Determining the geographical origins of natural emeralds through nondestructive chemical fingerprinting. *Journal of Gemmology*, **33**(1–4), 1–13, https://doi.org/10.15506/JoG.2012.33.1.1.

Cui, D., Liao, Z., Qi, L., Zhong, Q. & Zhou, Z. 2020. A study of emeralds from Davdar, north-western China. *Journal of Gemmology*, **37**(4), 374–392, https://doi.org/10.15506/JoG.2020.37.4.374.

DeWitt, J.D., Chirico, P.G., O'Pry, K.E. & Bergstresser, S.E. 2020. Mapping the extent and methods of small-scale emerald mining in the Panjshir Valley, Afghanistan. *Geocarto International*, article 1716394 (23 pp.), https://doi.org/10.1080/10106049.2020.1716394.

Forestier, F.H. & Piat, D.H. 1998. Emeraudes de Bactriane: Mythe ou réalité, La vallée du Panjshir (Afghanistan). *In*: Giard, D., Giuliani, G., Cheilletz, A., Fritsch, E. & Gonthier, E. (eds) *L'émeraude : Connaissances Actuelles et Prospectives*. Association Française de Gemmologie, Paris, France, 139–146.

Giard, D. 1998. Le Bouzkachi des émeraudes. Les émeraudes de la Vallée du Panjshir. *In*: Giard, D., Giuliani, G., Cheilletz, A., Fritsch, E. & Gonthier, E. (eds) *L'émeraude : Connaissances Actuelles et Prospectives*. Association Française de Gemmologie, Paris, France, 177–184.

Giuliani, G., France-Lanord, C., Zimmermann, J.L., Cheilletz, A., Arboleda, C., Charoy, B., Coget, P. *et al.* 1997. Fluid composition, δD of channel H_2O, and $\delta^{18}O$ of lattice oxygen in beryls: Genetic implications for Brazilian, Colombian, and Afghanistani emerald deposits. *International Geology Review*, **39**(5), 400–424, https://doi.org/10.1080/00206819709465280.

Giuliani, G., Chaussidon, M., Schubnel, H.-J., Piat, D.H., Rollion-Bard, C., France-Lanord, C., Giard, D. *et al.* 2000. Oxygen isotopes and emerald trade routes since antiquity. *Science*, **287**(5453), 631–633, https://doi.org/10.1126/science.287.5453.631.

Giuliani, G., Dubessy, J., Ohnenstetter, D., Banks, D., Branquet, Y., Feneyrol, J., Fallick, A.E. & Martelat, J.-E. 2017. The role of evaporites in the formation of gems during metamorphism of carbonate platforms: A review. *Mineralium Deposita*, **53**(1), 1–20, https://doi.org/10.1007/s00126-017-0738-4.

Giuliani, G., Groat, L.A. & Marshall, D.D. 2018. Emerald deposits in the 21st century: Then, now and beyond. *InColor*, No. 40, 22–32.

Giuliani, G., Groat, L.A., Marshall, D., Fallick, A.E. & Branquet, Y. 2019. Emerald deposits: A review and enhanced classification. *Minerals*, **9**(2), article 105 (63 pp.), https://doi.org/10.3390/min9020105.

Graham, D.J. & Midgley, N.G. 2000. Graphical representation of particle shape using triangular diagrams: An Excel spreadsheet method. *Earth Surface Processes and Landforms*, **25**(13), 1473–1477, https://doi.org/10.1002/1096-9837(200012)25:13%3C1473::aid-esp158%3E3.0.co;2-c.

Groat, L., Giuliani, G., Marshall, D. & Turner, D. 2014. Emerald. *In*: Groat, L.A. (ed) *Geology of Gem Deposits*, 2nd edn. Mineralogical Association of Canada Short Course Series, **44**, Québec City, Québec, Canada, 135–174.

Guillong, M. & Günther, D. 2001. Quasi 'non-destructive' laser ablation-inductively coupled plasma-mass spectrometry fingerprinting of sapphires. *Spectrochimica Acta Part B: Atomic Spectroscopy*, **56**(7), 1219–1231, https://doi.org/10.1016/s0584-8547(01)00185-9.

Hänni, H.A. 1980. *Mineralogische und mineralchemische Untersuchungen an Beryll aus alpinen Zerrklüften*. PhD thesis, University of Basel, Switzerland, 112 pp.

Henn, U. & Schmitz, F. 2014. Smaragde aus der Provinz Laghman, Afghanistan; ein Vergleich mit Smaragden aus dem Panjshir-Tal (Emeralds from Laghman Province, Afghanistan; a comparison with emeralds from Panjshir Valley). *Gemmologie: Zeitschrift der Deutsche Gemmologische Gesellschaft*, **63**(3–4), 105–110.

Hughes, R.W. 2021. Hyperion: The Lotus Gemology inclusion search engine. Lotus Gemology, Bangkok, Thailand, www.lotusgemology.com/index.php/library/inclusion-gallery, accessed December 2020.

Huong, L.T.-T. 2008. *Microscopic, chemical and spectroscopic investigations on emeralds of various origins*. PhD thesis, Johannes Gutenberg-Universität Mainz, Germany, 226 pp., https://doi.org/10.25358/openscience-2607.

Huong, L.T.-T., Häger, T. & Hofmeister, W. 2010. Confocal micro-Raman spectroscopy: A powerful tool to identify natural and synthetic emeralds. *Gems & Gemology*, **46**(1), 36–41, https://doi.org/10.5741/gems.46.1.36.

Karampelas, S., Al-Shaybani, B., Mohamed, F., Sangsawong, S. & Al-Alawi, A. 2019. Emeralds from the most important occurrences: Chemical and spectroscopic data. *Minerals*, **9**(9), article 561 (29 pp.), https://doi.org/10.3390/min9090561.

Kazmi, A.H. & Snee, L.W. (eds) 1989. *Emeralds of Pakistan: Geology, Gemology, and Genesis*. Van Nostrand Reinhold, New York, New York, USA, xii + 269 pp.

Krzemnicki, M.S. 2018. New emeralds from Afghanistan. *SSEF Facette*, No. 24, 12–13, www.ssef.ch/wp-content/uploads/2018/03/2018_SSEF_Facette_24.pdf.

Laurs, B.L. 2001. Gem News International: Emeralds from Laghman, Afghanistan. *Gems & Gemology*, **37**(1), 68.

Rossovskiy, L.N. 1981. Rare metal pegmatites with precious stones and conditions for their formation (Hindu Kush). *International Geology Review*, **23**, 1312–1320.

Rossovskiy, L.N., Chmyrev, V.M. & Salakh, A.S. 1976. New fields and belts of rare-metal pegmatites in the Hindu Kush (eastern Afghanistan). *International Geology Review*, **18**(11), 1339–1342, https://doi.org/10.1080/00206817609471351.

Sabot, B., Cheilletz, A., de Donato, P., Banks, D., Levresse, G. & Barrès, O. 2000. Afghan emeralds face Colombian cousins. *Chronique de la Recherche Minière*, No. 541, 111–114.

Sabot, B., Cheilletz, A., de Donato, P., Banks, D., Levresse, G. & Barrès, O. 2001. The Panjsher-Afghanistan emerald deposit: New field and geochemical evidence for Colombian style mineralisation. *European Union Geoscience XI, Strasbourg*, France, 8–13 April, 548.

Saeseaw, S., Pardieu, V. & Sangsawong, S. 2014. Three-phase inclusions in emerald and their impact on origin determination. *Gems & Gemology*, 114–132, https://doi.org/10.5741/gems.50.2.114.

Schmetzer, K. 2014. Letters: Analysis of three-phase inclusions in emerald. *Gems & Gemology*, **50**(4), 316–319.

Schmetzer, K., Schwarz, D., Bernhardt, H.-J. & Häger, T. 2006. A new type of Tairus hydrothermally-grown synthetic emerald, coloured by vanadium and copper. *Journal of Gemmology*, **30**(1/2), 59–74, https://doi.org/10.15506/jog.2006.30.1.59.

Schwarz, D. 2015. The geographic origin determination of emeralds. *InColor*, December, Special Issue: World Emerald Update, 98–105.

Schwarz, D. & Giuliani, G. 2002. Emeralds from Asia. *In*: Giuliani, G., Jarnot, M., Neumeier, G., Ottaway, T. & Sinkankas, J. (eds) *Emeralds of the World*. extraLapis English No. 2, Lapis International, East Hampton, Connecticut, USA, 60–63.

Schwarz, D. & Pardieu, V. 2009. Emeralds from the Silk Road countries: A comparison with emeralds from Colombia. *InColor*, No. 12, 38–43.

Schwarz, D. & Klemm, L. 2012. Chemical signature of emerald. *34th International Geological Congress*, Brisbane, Australia, 5–10 August, 2812.

Snee, L.W., Lindsay, C.R., Bohannon, R.G., Turner, K.J., Wasay, A., Omar, M., Seal, R.R., Wilds, S.R. *et al.* 2005. *Emerald Deposits of the Panjsher Valley, Afghanistan— Preliminary Assessment of Geologic Setting and Origin of the Deposits*. USGS Administrative Report 2005, Afghanistan Project Product No. 038, U.S. Geological Survey, Washington DC, USA, 97 pp.

Sosedko, T.A. 1957. The change of structure and properties of beryl with increasing amounts of alkalis. *Memoirs of the All-Union Mineralogical Society*, **86**, 495–499.

Sultan, M. & Aria, T. 2018. Afghanistan's emeralds: Hidden treasures. *InColor*, No. 40, 85–87.

Taran, M.N. & Rossman, G.R. 2001. Optical spectroscopic study of tuhualite and a re-examination of the beryl, cordierite, and osumilite spectra. *American Mineralogist*, **86**(9), 973–980, https://doi.org/10.2138/am-2001-8-903.

van der Maaten, L. & Hinton, G. 2008. Visualizing data using t-SNE. *Journal of Machine Learning Research*, **9**, 2579–2605.

Wang, H.A.O. & Krzemnicki, M.S. 2021. Multi-element analysis of minerals using laser ablation inductively coupled plasma time of flight mass spectrometry and geochemical data visualization using t-distributed stochastic neighbor embedding: Case study on emeralds. *Journal of Analytical Atomic Spectrometry*, preprint (10 pp.), https://doi.org/10.1039/d0ja00484g.

Wang, H.A.O., Krzemnicki, M.S., Chalain, J.-P., Lefèvre, P., Zhou, W. & Cartier, L. 2016. Simultaneous high sensitivity trace-element and isotopic analysis of gemstones using laser ablation inductively coupled plasma time-of-flight mass spectrometry. *Journal of Gemmology*, **35**(3), 212–223, https://doi.org/10.15506/JoG.2016.35.3.212.

Winchell, A.N. & Winchell, H. 1951. *Elements of Optical Mineralogy*, Part 2. John Wiley & Sons Inc., New York, New York, USA, 551 pp.

Wood, D.L. & Nassau, K. 1968. Characterization of beryl and emerald by visible and infrared absorption spectroscopy. *American Mineralogist*, **53**(5–6), 777–800.

The Authors

**Dr Michael S. Krzemnicki FGA[1,2],
Dr Hao A. O. Wang[1] and Susanne Büche[1]**

[1] Swiss Gemmological Institute SSEF, Aeschengraben 26, 4051 Basel, Switzerland

[2] Department of Environmental Sciences, University of Basel, Switzerland

Email: michael.krzemnicki@ssef.ch